Steel-to-concrete connections in narrow concrete corners

A numerical study into calculation simplifications for asymmetric joints and its impact on design

Daniel Carlson Bjernald & Emil Lönn

1st of June 2022

Abstract

A commonly occurring problem when designing steel-to-concrete connections in corners with space deficits is the necessity for irregularly placed bolts with regards to design codes. The complexity of the calculations for the irregular placements of bolts generates the need to use simplified models during the design. This simplification could lead to differences between the design and the physical product, resulting in uncertainties regarding the connection's strength. The purpose of this thesis is to enhance the understanding of the effects on strength and the modes of failure for the connection due to the simplified models used and investigate whether the geometrical changes could be accounted for in design.

The study was performed using numerical analysis to simulate the real life behaviour of two models subjected to relevant load effects. The models were constructed in the finite element software Abaqus and validated as well as calibrated against laboratory tests performed at Luleå Technical University in 2013. The extent of the study was limited to a single case of simplified design with no regards to concrete reinforcement and tested in isolation from the entirety of the structure by the use of boundary conditions.

Results show the existence of a reduction in capacity for the irregular shaped connection compared to the design model and changes to the associated failure mode. However, further studies and parametrization is needed to find conclusive evidence that the found relations are relevant for the general case and could be used for future design.

Sammanfattning

Ett vanligt förekommenade problem vid utformning av stål-och betonganslutningar i hörn är att platsbrist kan ge upphov till anslutningar som är asymmetriskt utformade. De avvikande placeringarna på bultarna medför komplexa beräkningar och skapar ett behov av förenklade modeller vid design. Förenklingen kan leda till skillnader i brottsbeteende mellan designen och den fysiska produkten vilket kan leda till osäkerheter kring anslutningens hållfasthet. Syftet med den här avhandlingen är att öka förståelsen för förenklade beräkningsmodellers inverkan på anslutningens hållfasthet och brottmod samt undersöka huruvida geometriska skillnader kan beaktas i design.

Studien genomfördes som en numerisk analys av två modellers verkliga beteende under påfrestan av relevanta lasteffekter. Modellerna konstruerades i finita elementprogrammet Abaqus och valideras samt kaliberades mot laboratoriska försök utförda vid Luleå tekniska universitet under 2013. Studiens omfattning avgränsades till ett enskilt fall av en förenklad modell utan beaktning av möjlig armering och testades i avskildhet utan interaktion med övriga konstruktionen med hjälp av randvillkor.

Resultaten påvisade förekomsten av kapacitetsbrist i anslutningen med avvikande bultplacering i förhållande till den förenklade modellen samt möjliga förändringar av dess brottsmod. Vidare studier och parametrisering krävs emellertid för att finna uteslutande bevis för att upptäckterna kan styrkas för det generella fallet och kan användas i framtida utformning.

Förord

Med detta examensarbete närmar sig slutet på vår fem år långa utbildning vid Lunds Tekniska Högskola. Vi vill först och främst tacka våra handledare Fernando och Rasoul ifrån AFRY samt Ivar för att ha hjälpt oss kontinuerligt i diskussioner och stunder då vi hade det som allra svårast. Tack för att ni stått ut med oss och alla våra frågor. Ett särskilt tack ska också riktas till Ahmed Elkady som bidrog med oerhört mycket kunskaper om datorprogrammet som användes i detta examensarbete.

De fem gångna åren har varit något utav det roligaste i våra liv samtidigt som vi träffat vänner för livet som vi gärna vill rikta ett stort tak till, utan er hade vi inte varit här idag! Nu ser vi båda fram emot ett spännande liv framför oss som civilingenjörer och vi hoppas att detta arbete bidrar till kunskapen om stål-betonganslutningar inom yrket.

Daniel Carlson Bjernald
Emil Lönn

Notations and Symbols

Latin letters

$A_{c,N}$ - Actual projected area
$A^0_{c,N}$ - Reference projected area
A_s - Anchor bolt tensile stress area
A_h - Bearing area of an anchor's head
d_h - Diameter of the head of a headed fastener
d_u - Diameter of an anchor
c - Edge distance from the axis of a fastener
$c_{cr,N}$ - Characteristic edge distance for ensuring the transmission of the characteristic resistance of a single fastener case of concrete break-out under tension load
C_{Ed} - Resultant compression force between fixture and concrete
E - Young's modulus
e_N - Eccentricity of resultant tension force of tensioned fasteners
$f_{c,cu}$ - Compressive cube strength
$f_{c,cy}$ - Characteristic compressive cylinder strength
f_t - Tensile stress
f_u/f_{ub} - Ultimate tensile stress
f_y - Yield stress
G - Fracture energy
h_{ef} - Effective embedment depth
N_{Ed} - Design tension force
$N_{Rd,c}$ - Design resistance, concrete cone failure
$N_{Rk,c}$ - Characteristic resistance, concrete cone failure
$N^0_{Rk,c}$ - Characteristic resistance of a single fastener not influenced by other fasteners in $N_{Rk,s}$ - Characteristic steel resistance of a fastener under tension load
$N_{Rk,p}$ - Characteristic resistance in case of pull-out failure
$N_{Rk,sp}$ - Characteristic resistance in case of concrete splitting failure
its surroundings or by the distance from the concrete edges
s - Centre to centre spacing of fasteners in group
$s_{cr,N}$ - Characteristic spacing of fasteners to ensure characteristic resistance of the fastener or group of fasteners in case of concrete cone failure
w - Crack width z - Internal lever arm

Greek letters

ε - Strain
$\epsilon_c{}^{in}$ - Inelastic strain, compression
$\epsilon_t{}^{in}$ - Inelastic strain, tension
$\epsilon_c{}^{pl}$ - Plastic strain, compression

$\epsilon_t{}^{pl}$ - Plastic strain, tension
γ_{Mc} - Partial factor for concrete cone failure
σ - Stress
σ_2 - Confinement stress
$\Psi_{ec,N}$ - Factor taking into account for group effect when different tensions loads are applied in case of concrete cone failure
$\Psi_{h,sp}$ - Factor taking into account the influence of the member thickness on the splitting resistance
$\Psi_{M,N}$ - Factor taking into account for the compression force between connection and concrete that originates from bending moment with or without axial forces
$\Psi_{re,N}$ - Shell spalling factor
$\Psi_{s,N}$ - Factor taking into account the disturbance of stress distribution that occurs due to proximity of an concrete edge in case of concrete cone failure

Glossary

$HFRHS$ - Hot Formed Rectangular Hollow Section

Contents

1 Introduction

In this introduction chapter the background, purpose and method of the thesis will be addressed. Limitations that were necessary for the scope of the thesis will also be presented. A general overview of the master thesis structure is presented last.

1.1 Background

The conventional method of designing joints between a steel plate and concrete is to have a square or rectangular shaped steel backing plate. The goal for the joint is to achieve a moment-resistant connection that fulfills serviceability critera (SLS) as well as the ultimate limit state (ULS). There is good knowledge of these connections due to its prevalence in load-bearing structures making them described in detail in design guides. However, in some scenarios where there might not be enough room for a symmetrical steel plate connection due to the concrete corner being to narrow e.g. Such as in lift shafts, a modified and asymmetrical connection may be used. In this case, due to the complexity of the required calculations, there might be advantages in designing the connection according to a standard model found in the design codes. Both the standard and the narrow corner connection are illustrated in Figure 1.1 and will for the remainder of this thesis be referred to as such.

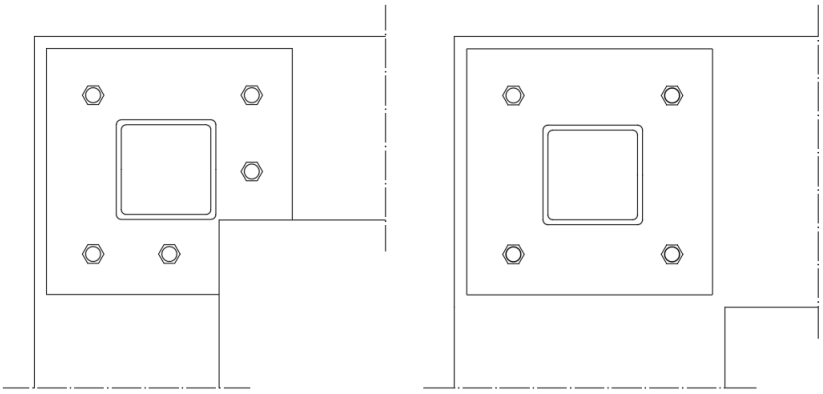

Figure 1.1: Narrow corner connection (left) and the standard (right).

1.2 Purpose and method

The purpose of this Master thesis was to study how the geometrical changes of a narrow steel-to-concrete connection affects its capacity when subjected to common static load effects and investigate how a narrow model could be used in future design of similar joints. To better understand the behaviour of the connections, investigation into the expected failure modes will be performed.

The finite element method (FEM) was used in order to investigate the problem with considerations for the non-linear behaviour of concrete. By the usage of the FE-software *ABAQUS CAE* the two connections shown in figure 1.1 could be modelled and tested for the different load cases. By applying the same load on both models, comparisons could in the end be made between the two regarding their expected behaviour and maximum capacity in the anchors. To be sure that the behaviour of the concrete is captured, a validation of the model was first conducted. Material properties used for validation and calibration of the model was collected from laboratory experiments. Validation and calibration to a satisfactory level was thereafter achieved by matching the results with the tested values from the same experiments.

To further investigate the failure modes achieved during loading, relevant design codes was used to compare the tested maximum capacity with theoretical values. This was used to provide an explanation and help draw conclusions regarding the results.

1.3 Limitations and assumptions

Due to the time given for this master thesis, some limitations are necessary for the scope.

- A specific type of narrow cornered connection was considered.
- No lab experiments were executed.
- It is assumed that the fixture is in direct contact with the concrete. This could be achieved using grout or another type of filling. They are however assumed to have no impact on the bearing of the structure.
- The connection in question was studied separately and not as a part of the greater structure. This was done by applying boundary conditions to the edges of an arbitrary section where negligible effect on the analysis is expected.
- The influence of reinforcement in the concrete is not a part of this analysis.

1.4 Thesis overview

This section describes the different chapters to give an overview of the structure of the thesis.

Chapter 2 presents general theory found in literature on anchoring and its failure modes as well as the behaviour of steel and concrete.

Chapter 3 displays the design requirements governing the design of the type of steel-concrete connections investigated in this study. It covers the relevant Eurocode chapters and researched models for describing serviceability limits for elevators.

Chapter 4 describes the pre-processing input data for the finite element model and presents the relevant material models used for analysis.

Chapter 5 presents the result of the model calibration where the model parameters are compared with experimental values.

Chapter 6 presents the static analysis implemented on the studied joints as well as the results and a comparison with the values found in literature.

Chapter 7 concludes the findings and discusses possible uncertainties in the study. Additionally, topics for extended development and improvement of this study, as well as suggestions for further studies, are presented.

2 Steel anchorage in concrete

Anchoring of steel structural components is commonly achieved by fastening an end plate to the concrete structure with the use of anchor-bolts. The purpose of the fasteners is to transfer loads from the secondary structure to the main component, which in this case is from the steel columns to the concrete. The mechanism which transfers the load between the anchor-bolts and the concrete are most commonly mechanical interlock, friction or chemical bond. [1]

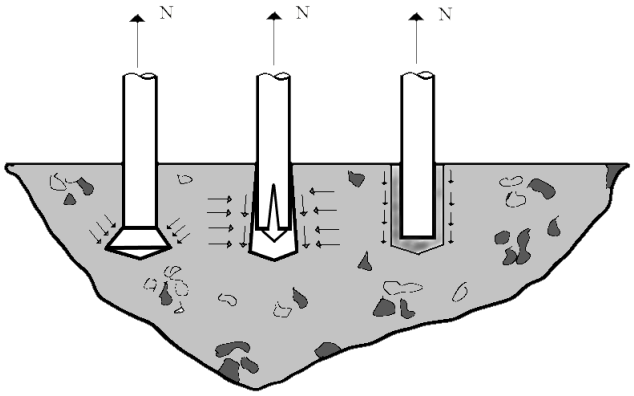

Figure 2.1: Illustration of mechanical interlock(left), friction(middle) and chemical bond(right) between steel fastener and concrete.

Anchorage systems are usually divided into cast-in-place and post-installed anchors. By installing the fasteners in the formwork prior to pouring of the concrete the cast-in-place system is achieved. Examples of this solution is headed anchors and welded headed studs. Post-installed anchorages are installed by drilling holes into the hardened concrete and inserting the fasteners into them. For example mechanical expansion or adhesive anchors are commonly used post-installed systems. [1]

The most used mechanism is mechanical interlock for both cast-in-place and post-installed anchorage systems. It transfers load by the usage of bearing interlocks between the two components. The friction mechanism is obtained by using expansion anchors. An expansion force is induced which generate friction between the fastener and concrete. This friction force is in equilibrium with the external tensile force. Chemical bond anchorages use an adhesive bond in order to transfer the load to the concrete base. [1]

2.1 Behaviour of Hot-rolled Steel

Any material that is classified as steel consists of alloys of iron with less than 2% carbon content. Steel is made out of iron ore that together with limestone and coal fragments are melted to create the material. It is an isotropic material which means that it is equally strong in different directions, in tension and (locally) compression [2].

The stress-strain behaviour of structural steel under tensile load is idealized in figure 2.2. Initially, the stress-strain curve is linear where the slope is equal to Young's modulus E according to Hooke's law, $E = \sigma/\varepsilon$ where E is 200-210 GPa for steel. In the linear elastic stage the material remains elastic which means that the deformations recovers when it is unloaded again.

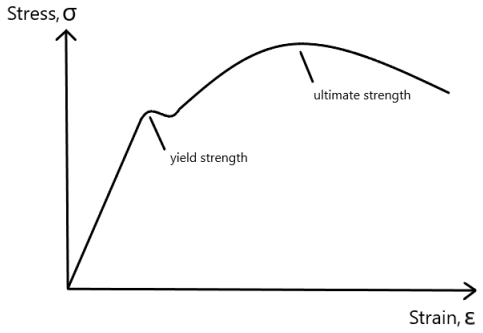

Figure 2.2: Illustration of the stress-strain diagram of steel.

When it reaches the yield stress f_y the limit for the elastic behaviour is reached and the material flows without any increase in the stress. During this state steel deforms plastically which means that a portion of the deformations in the material remains when it is unloaded. When the strain-hardening strain ε_{cs} is reached the stress increases above yield stress f_y until the ultimate tensile stress f_u is reached. The load capacity decreases from here until fracture occurs due to local reductions in the cross section [2].

The yield stress and ultimate tensile stress are associated to the steel quality and the dimensions of the cross sections. For mild structural steel the most common steel qualities are S355, S275 and S235 where f_y is between 235 and 355 MPa depending on thickness and f_u is in the range 360-470 MPa [3].

2.2 Behaviour of Concrete

Concrete is a composite material consisting of aggregates and a mortar matrix. The combination of multiple materials entails a heterogeneous loading response in the concrete, which depends not only on the individual materials but also the interaction between them. This means that the behaviour of concrete varies between different principal stress directions depending on load conditions. Many experiments have been

conducted to study its behaviour and ultimate stress methods for concrete in compression, tension and multiaxial stress states have been developed. These are used to determine the shape of the load-displacement curve. [4]

Concrete is a composite material which, in its most generalized form, is composed of cement, sand, water and aggregate. The material is characterized by its uni-axial strength where it has high strength in compression and its tensile strength is about a tenth of its compressive capacity. To prevent complete failure in regions loaded in tension the most common approach is by the use of cast-in reinforcement bars. By changing the amount of reinforcement, the moment capacity and general strength of the material can be vastly altered. Thanks to its high capacity and low cost compared to other building materials concrete is the most common building material and is used in all forms of load-bearing constructions [5].

In the following subsections the physical phenomena of microcracking in the concrete affect the macroscopic stress-strain relations. Microcracks are very small cracks in the bond that propagate through the cementitious matrix without resulting in a reduced stiffness. They are mainly initiated as a result of incomplete hydration and drying shrinkage as well as different nonmechanical loading situations. [6]

2.2.1 Compressive behaviour

When unconfined concrete is subjected to uniaxial compressive loads, it displays highly non-linear behaviour with a failure mode characterized by a critical degree of microcracking. This failure mode is brittle in its nature, as shown in figure 2.3. The initial response when subjected to approximately 30% of the compressive strength shows that the cracks do not increase and the stress-strain curve is considered linear. Upon further loading to about 70-75% cracking starts to occur parallel to the load direction, resulting in the non-linear behaviour depicted. The macroscopic stiffness in the material is reduced even though it is considered marginal in this stage. These cracks continue to propagate until the appearance of macroscopic cracks in the test sample once the ultimate strength have been reached. After reaching maximum stress, the curve descends in what is referred to as the *softening phase*. At this stage crushing failure occurs at the ultimate strain. [6]

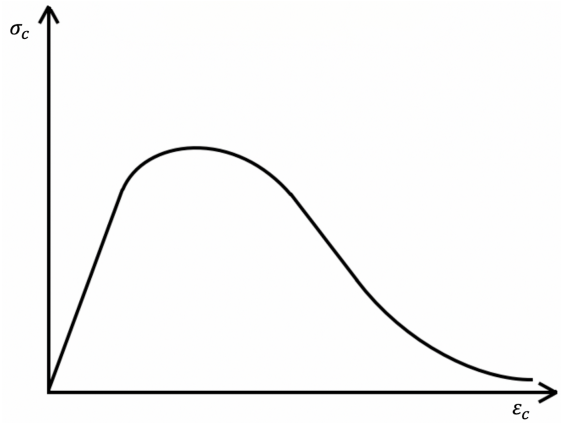

Figure 2.3: Compressive behaviour of concrete in stress-strain.

2.2.2 Tensile behaviour

The tensile behaviour of concrete is more uncertain and difficult to carry out compared to for compressive load testing because of the difficulty of finding an anchor point that does not interfere with the test. Multiple test approaches exist, including a four point loading test. The result from one of those test in the form of a stress-strain diagram is shown in figure 2.4. If integrated, the area under the curve measures the total amount of fracture energy [Nm/m2] developed, which is the energy needed to produce a crack.

Figure 2.4: Tensile behaviour of concrete in stress-strain.

When applying a tensile load, a linear relation can be studied up to approximately 60% of the ultimate tensile strength. In this interval no microcrack propagating occurs. Beyond this point, additional microcracks starts to appear and the loading curve deviates from the linear path. This results in a stiffness reduction which will increase up until just before the tensile strength is reached. At this point and upon further loading the cracks have formed a continuous pattern in the entire specimen. The cracks appear orthogonal to the load direction and form in a localized zone, unlike for the compression tests where the cracks are parallel to the load. This result in a rapid decrease of strength. [6] Since the cracks only appear in the cement paste, they will result in an irregular shape governed by the position of the aggregate and not a straight line. This phenomenon increases the strength by introducing shear resistance in the direction on loading. [7]

2.2.3 Multiaxial stress states

It is shown that concrete generally is a brittle material when subjected to compressive and tensile stresses. However, when subjected to high multiaxial stresses it shows a more ductile behaviour as shown in figure 2.5, depending on the loading conditions. Such behaviour may be realized with the addition of confining stirrups which, when used for instance in columns, will improve the deformation capacity of the confined concrete substantially. When a higher compressive confinement stress σ_2 is added, the ductility of the material increases.

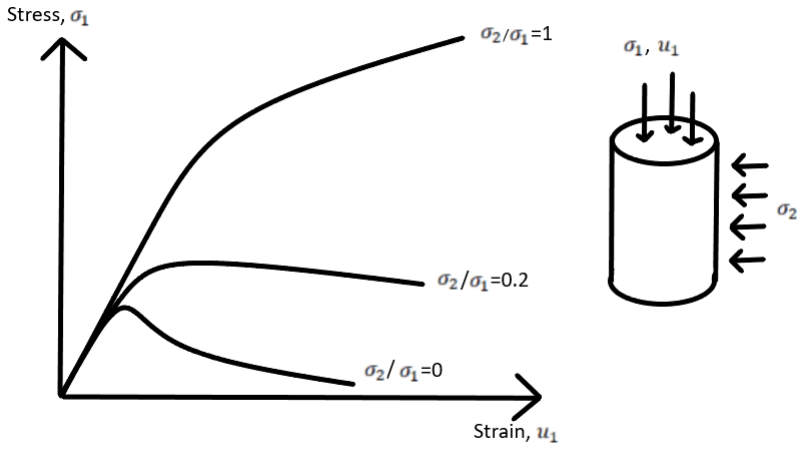

Figure 2.5: Stress-strain diagram depicting the confinement stress relations impact on concretes general behaviour.

A ductile material has a higher ability to redistribute stress concentrations and therefore increase its capacity. The interaction between the two principal stresses cooperate, resulting in a possible increase of strength totaling approximately 16%, as seen in figure 2.5 [7]. This does however not apply for multiaxial tensile stress state which closely resemble the uniaxial case. For the case of biaxial stress states as displayed in figure 2.6, when tensile principal stresses and compressive principal stresses coincide, a reduction of strength can be seen. [6]

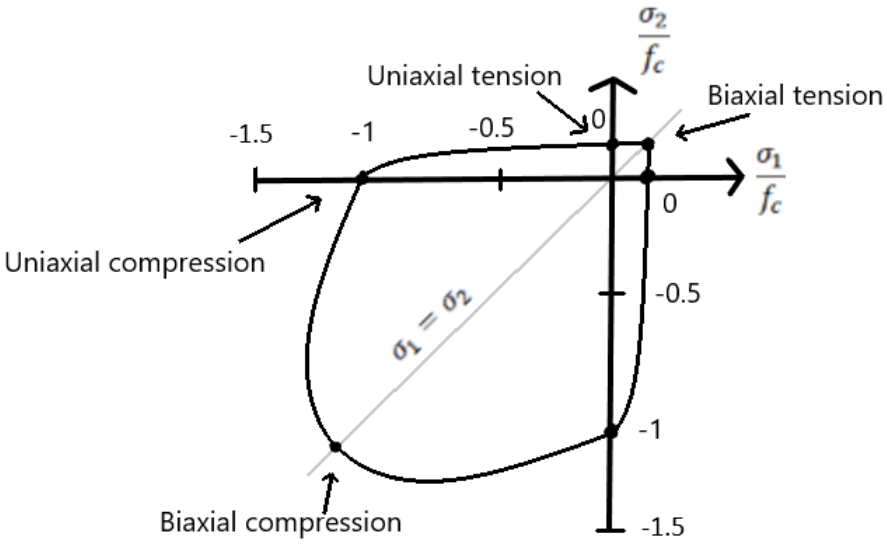

Figure 2.6: Bi-axial stress states for concrete. [7]

2.2.4 Non-linear material models of concrete

For the application of concrete material behaviour in solving engineering problems, several approaches have been developed. The most easily applicable approach considers a linear-elastic model in which it is possible to verify the existence and magnitude of failure modes to compare with design values. It is however in complex cases, or especially when analysing existing structures, important to define non-linear material models to fully evaluate the effect of the loading on the material. [7]

Two constitutive approaches exist to describe cracking of concrete for finite element analysis; the continuum-based approaches and discrete cracking approaches. The fundamental difference is in the way the occurrence of cracks is represented within the model. A continuum model describes both the elastic behaviour as well as the behaviour of the crack within each element. The behaviour is therefore continuous over element boundaries and crack propagation is taken into consideration in the material properties of each element. In contrast to the continuum approach, the discrete model creates physical cracks in the model while the element stiffness is fully linear. [6]

A common problem with discrete approaches is that for the modelling, the loaction of cacks must be known beforehand, which could result in misleading analysis's. In this report a continuum approach will be adopted. Due to the complexity of the behaviour of concrete, extensive work has been conducted over the years to realistically describe its macroscopic behaviour. A continuum based model to describe the evolution of damage from pre-failure to post-failure using plasticity, damage theory and fracture mechancis (called the plastic damage model) was proposed in 1989 by Lubliner et. al and serves as the base for the finite element analysis material model used in this thesis.

Plasticity is a concept to consider the effects of yielding of materials and is generally very useful for materials such as steel. It has however been found to be useful for finite element analysis of brittle structures under certain circumstances. In cases where tensile loads are applied in a concrete material, plastic theory can successfully approximate the behaviour in the compressive zones while fracture mechanics is used for zones where at least one principal stress is tensile. The formulation of plasticity follows three essential concepts; yielding, hardening and a flow rule.

2.3 Failure modes

For fasteners loaded in tension there are a couple of failure modes which can happen. These depend on a number of parameters deciding the cause of failure. For anchors loaded in tension, which is the case in this study, there are four failure modes that can happen and will be explained in this section [1].

2.3.1 Pull-out failure

Pull-out failure is determined by the strength that is holding the fastener together with the concrete. When this failure happens, the anchor is pulled out from the hole as illustrated in Figure 2.7. As can be seen in the illustration, it is also possible that the concrete is locally damaged. For expansion anchors this occurs when the expansion force holding the anchor in place is insufficient resulting in a loss of friction.

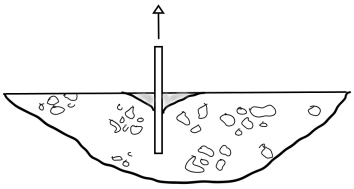

Figure 2.7: Illustration of a pull-out failure.

2.3.2 Concrete cone failure

Concrete cone failure occurs when the tensile capacity in the concrete is reached thanks to the fasteners having enough capacity to resist pull-out failure. When this failure mode occurs, as suggested by the name, the concrete has a cone-shaped fracture which is shown in Figure 2.8. The angle of the cone is most commonly between 30 and 40 degrees with indications from previously conducted tests that the angle increases with embedment depth [1].

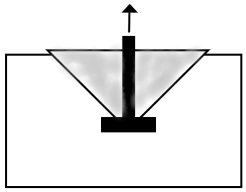

Figure 2.8: Illustration of a concrete-cone failure according to Eurocode.

The capacity for concrete cone failure is affected by the placement of anchors and its distance to nearest concrete edge. For anchors that are placed closely together there is a risk of an aggregated cone breakout. The placement of anchors near the concrete edge can also trigger a breakout involving the cone. A local blow-out failure of the concrete can happen for anchors and studs which are placed close to the edge[1]. Eurocode deals with the problem of spacing and distance to nearest edge with different safety factors which will be handled later in the report.

2.3.3 Splitting failure

Splitting failure is self-explanatory since the concrete around a fastener loaded in tension splits, see Figure 2.9. It occurs due to concrete dimensions being too small or that the spacing between anchors is too low. Also, having anchors close to the edge increases the risk of splitting failure [1].

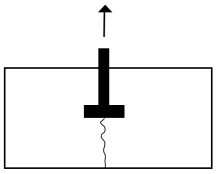

Figure 2.9: Splitting failure as illustrated by Eurocode.

2.3.4 Local side blow-out failure

A local side blow-out failure, or just blow-out failure, is a failure mode in which the edge distance is nonsufficient in preventing cracking while the embedment depth of the anchor is large enough to prevent concrete cone failure. This failure mode is mostly relevant for pre-installed anchors because of the large splitting risk during installation for post-installed anchors due to high torque. Figure 2.10 presents the physical appearence of the failure mode which in nature is different than most other failures due to tension in the bolts considering it has a lateral crack pattern, perpendicular to the normal force applied. It is caused by the quasi-hydrostatic pressure buildup in the area which generate a lateral bursting force F_b. This force is related to the normal force by a factor α which depends on the specific concrete bearing pressure beneath the bolt head. This is because the lateral strain in the concrete increases with the stress beneath.

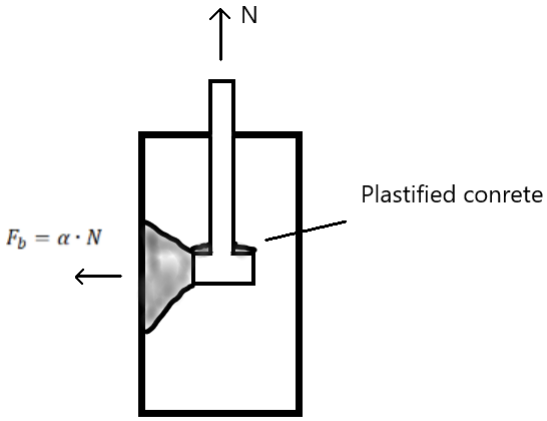

Figure 2.10: Blow-out failure as illustrated by Eligehausen. [1]

2.3.5 Steel failure

For anchors with a deep embedment depth loaded in tension, the capacity for the concrete might be so high that the most critical failure mode concerns failure of the steel or bolts. Due to this high capacity this is the most unusual failure mode of the four mentioned.

Thanks to the desire of maximising load capacity for a given embedment depth concrete cone is the most common failure mode for anchors loaded in tension. A comparison of the mentioned failure modes is observed in Figure 2.11.

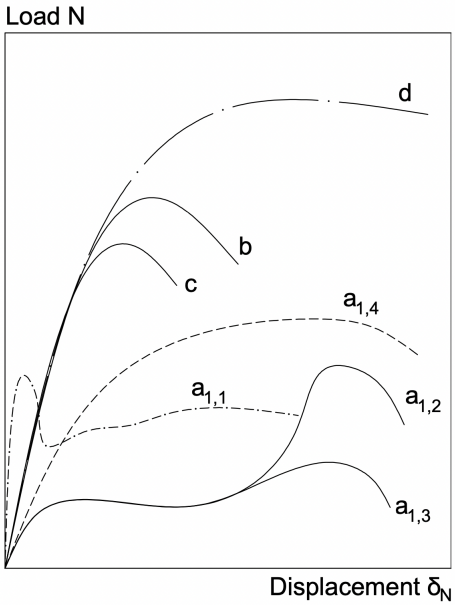

Figure 2.11: Load-displacement curves for mentioned failure modes.(Eligehausen et al. 2006)

Curve a_{1-4} illustrates load-displacement curves for different types of pull-through failure which depends on design choices made regarding anchor type and how it is connected to the concrete. Curve c represents splitting failure, b represents cone failure and d represents steel failure. Failure due to concrete splitting is less common since it is mostly avoided by following the requirements stipulated in Eurocode for minimum spacing and edge distance. As can be observed from the figure, steel and pull-out failure are subject to large deformations at their maximum load. Because of this they are regarded as ductile failure modes while cone and splitting exhibit smaller deformation and are seen as brittle failure modes.

3 Design requirements

Many different design standards for construction have been produced and are implemented throughout the world. In Europe, the harmonised standards for structural design called Eurocode are the ones primarily used and can be identified by its prefix; EN. A harmonised standard is recognised by and produced following a request by the European Commission to one of the European Standards Organisations. They can be used to demonstrate that the specified product and process are in compliance with relevant EU legislation.

Beyond the Eurocodes, alternative such as the design codes produced by Fédération internationale du béton (fib) can be used. Fib is a non-profit association committed to improving the technical, economic, aesthetic and environmental performances of concrete structures worldwide. Both codes present similar approaches on design which are based on mainly the same research but provides different interesting takes, useful for broadening the perspective of this thesis. Considering the design of concrete anchorage, both codes present a strictly elastic analysis, compulsary when brittle failure of the conncetion is expected. However, if the assumed failure mode is a ductile steel failure in the anchor, a plastic analysis could be performed, in which significant redistrituion of tension and shear in a group is assumed. This chapter presents both the design codes starting with Eurocode SS-EN 1992-4:2018 and followed by fib Bulletin 58.

3.1 Eurocodes

For design of anchorage in concrete in the ultimate limit state, the relevant requirements are found in Eurocode SS-EN 1992-4:2018 chapter 7. Six required verfications of failure modes for headed and post-installed fasteners in tension is specified. As the focus of this study only considers pre-installed headed anchors, the relevant modes are, as numbered in the original documents:

1 Steel failure

2 Concrete cone failure

3 Pull-out failure

5 Concrete splitting failure

6 Concrete blow-out failure

A distinction is also made for when the concrete is equipped with supplementary reinforcement, in which case two further failure modes is relevant. They are:

7 Steel failure of reinforcement

8 Anchorage failure of reinforcement

Reinforcement in the concrete was however not considered in this study and will therefore not be of further interest.

3.1.1 Steel failure of fastener

The characteristic tensile steel resistance is based on the ultimate tensile strength of the bolt and is determined as in equation 3.1 according to SS-EN 1993-1-8:2005 – Cl. 3.6.1. (3).

$$N_{Rk,s} = 0.9 f_{ub} A_s \qquad [N] \tag{3.1}$$

where

f_{ub} is the ultimate tensile strength of the bolt. [MPa]

A_s is the anchor bolt tensile stress area. $[mm^2]$

3.1.2 Concrete cone failure

Several models developed through theoretical and experimental studies have been used to describe the failure mechanisms of cast-in-place headed anchors loaded in tension. The model used in SS-EN 1992-4 and explained in this section is called the *Concrete Capacity Method* or *CC-Method*, which is widely implemented in European and US design guides. It is, however, referred to as the *Concrete Capacity Design Method* or *CCD-Method* in the US. [8] The method is a more practical solution to assess the failure loads of anchors compared to earlier methods due to its empirically derived equations. [1]

Because of the empirical background of the CC-method and the simplified assumptions that the member thickness, surface reinforcement and size of the anchor bearing have negligible effects on anchorage capacity and performance, the method might underestimate or overestimate the failure load of headed anchors if they differ appreciably from those tested. This is accounted for in the code by setting specific requirements for geometry of the fasteners designed. The scope of the thesis does not, however, include these applications and it is therefore not further considered.

The required verification for fasteners loaded in tension in regards to concrete cone failure according to section 7.2.14 in SS-EN 1992-4:2018 is described in equation 3.2.

$$N_{Ed} \leq N_{Rd,c} = \frac{N_{Rk,c}}{\gamma_{Mc}} \qquad [N] \tag{3.2}$$

where

N_{Ed} $= N_{Ed}^{g}$ for a group of fasteners.

$N_{rD,C}$ is the design tensile resistance.

γ_{Mc} is the partial factor for concrete cone failure mode.

The characteristic resistance of a single anchor or a group of anchors is determined using equation 3.3.

$$N_{Rk,c} = N_{Rk,c}^{0} \cdot \frac{A_{c,N}}{A_{c,N}^{0}} \cdot \Psi_{s,N} \cdot \Psi_{re,N} \cdot \Psi_{ec,N} \cdot \Psi_{M,N} \qquad [N] \tag{3.3}$$

where the factors are given individually below.

The characteristic resistance of a single fastener not influenced by other fasteners in its surroundings or by the distance from the concrete edges $N_{Rk,c}^{0}$ is determined as described in equation 3.4. In equation 3.4, the factor k_1 is dependent on whether the concrete is cracked or not and the variables dependant on that are given in the corresponding European Technical Product Specification. The values presented here are the indicative values.

$$N_{Rk,c}^{0} = k_1 \cdot \sqrt{f_{ck}} \cdot h_{ef}^{1,5} \qquad [N] \tag{3.4}$$

where

k_1 $= k_{cr,N} = 8,9$ for cracked concrete [-]

$= k_{ucr,N} = 12,7$ for uncracked concrete [-]

h_{ef} is the effective embedment depth [mm]

f_{ck} is the nominal characteristic compressive cylinder strength [MPa]

The geometrical effect of axial spacing and edge distance is taken into account by the value determined in equation 3.5.

$$A_{c,N}/A_{c,N}^{0} \qquad [-] \tag{3.5}$$

where

$A_{c,N}$ is the actual projected area, see figure 3.1 for an example. It is limited by overlapping concrete cones of adjacent fasteners ($s \leq s_{cr,N}$), as well as by edges of the concrete member ($c \leq c_{cr,N}$). $[m^2]$

$A_{c,N}^{0}$ is the reference projected area ($= s_{cr,N} \cdot s_{cr,N}$), see figure 3.2. $[m^2]$

and

$s_{cr,N}$ is the characteristic spacing of fasteners to ensure the characteristic resistance of the individual fasteners in case of concrete cone failure under tension load. [mm]

$c_{cr,N}$ 2cm is the characteristic edge distance for ensuring the transmission of the characteristic resistance of a single fastener in case of concrete break-out under tension loading, given by $s_{cr,N} = 2c_{cr,N} = 3h_{ef}$.

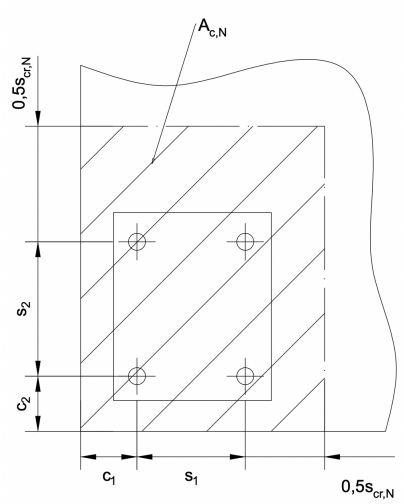

Figure 3.1: An example of an actual area $A_{c,N}$ of the idealized concrete cone for a group of fasteners, re-illustrated from SS-EN 1992-4:2018. [9].

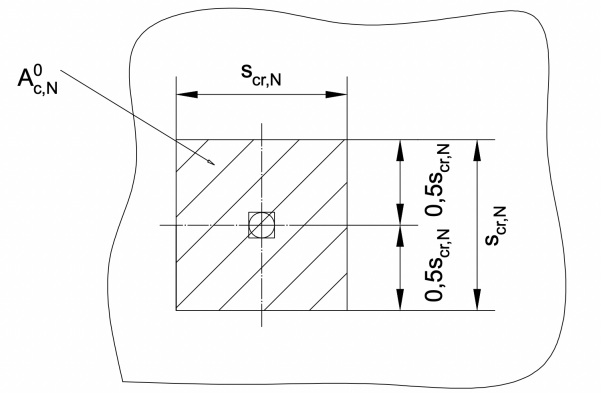

Figure 3.2: Idealized area $A^0_{c,N}$ of an idealized concrete cone of an individual fastener as presented in SS-EN 1992-4:2018. [9].

The disturbance of distribution of stresses in the concrete due to proximity to an edge is accounted for in equation 3.6.

$$\Psi_{s,N} = 0,7 + 0,3 \cdot \frac{c}{c_{cr,N}} \leq 1 \qquad [-] \tag{3.6}$$

where

c is the edge distance from the axis of a fastener. If several fasteners are present, the closest distance is used. [mm]

$c_{cr,N}$ is as described in equation 3.5. [mm]

When there is densely placed reinforcement present and when the effective embedment depth (h_{ef}) is lower than 100 mm, the effect of shell spalling is considered. This is done according to equation 3.7 in which the shell spalling factor is determined.

$$\Psi_{re,N} = 0,5 + \frac{h_{ef}}{200} \leq 1 \qquad [-] \tag{3.7}$$

where

h_{ef} is the effective embedment depth. [mm]

The factor $\Psi_{re,N}$ may however be taken as 1.0, in the following two cases:

1. Reinforcement is present at spacing $\geq$ 150 mm.
2. Reinfocrement with a diameter of $\leq$ 10 mm is present at spacing $\geq$ 100 mm.

The effect of a group of fasteners with different tension loads acting on them are accounted for using equation 3.8. The difference in tension load is accounted for with an eccentricity between the geometric centre of gravity of the tensioned fasteners and the point of resultant tensile force of tensioned fasteners.

If the eccentricity is biaxial, the product of the two factors determined in equation 3.8 based on the two eccentricities is used in equation 3.3.

$$\Psi_{ec,N} = \frac{1}{1 + 2 \cdot (e_N / s_{cr,N})} \leq 1 \qquad [-] \tag{3.8}$$

where

e_N is the eccentricity of resultant tension force of tensioned fasteners in respect to the centre of gravity of the tensioned fasteners. [mm]

$s_{cr,N}$ is as described in equation 3.5. [mm]

When a bending force is acting on the joint and a resulting compressive force is present, the factor determined in equation 3.9 is applied. The factor can be determined in two ways as follows:

(3.9)

1. $\Psi_{M,N} = 1.0$
   if
   - fastenings have an edge distance of $c < 1.5h_{ef}$;or
   - fastenings with $c \geq 1.5h_{ef}$ are loaded by a bending moment and a tension force with $C_{Ed}/N_{Ed} < 0.8$; or
   - fastenings with $z/h_{ef} \geq 1.5$.
2. $\Psi_{M,N} = 2 - \frac{z}{1.5h_{ef}} \geq 1$ for all other cases. $[-]$

where

C_{Ed} is the resultant compression force between fixture and concrete (taken as absolute value). [N]

N_{Ed} is the resultant tension force of the tensioned fasteners. [N]

z is the internal lever arm of a fastening calculated according to the theory of elasticity. [mm]

3.1.3 Pull-out failure of fastener

The characteristic resistance of pull-out failure for a headed fastener is determined using equation 3.10. For other types of fasteners, the resistance must be guaranteed by manufacturer. The formula presented only applies for circular heads.

$$N_{Rk,p} = k_2 \cdot A_h \cdot f_{kc} \qquad [kN] \tag{3.10}$$

where

k_2 = 7.5 for cracked concrete

= 10.5 for uncracked concrete

A_h is the bearing area of anchor's head

$= \frac{\pi}{4}(d_h^2 - d_a^2)$

d_h is the diameter of the head of a headed fastener. [mm]

d_a is the diameter of an anchor. [mm]

f_{ck} is the characteristic concrete compressive cylinder strength. [MPa]

and d_h should not be taken larger than $6t_h + d_a$

3.1.4 Concrete splitting failure

Two types of failure scenarios are considered in SS-EN 1992-4:2018 regarding concrete splitting failure; failure during installation due to torque applied to a fastener and failure due to loading. The first one could be avoided by applying minimum spacing requirements as well as following requirements for reinforcement. Failure due to loading will be presented in this chapter and is taken into consideration using a member thickness variable in the design codes similar to those for concrete cone failure. It is however rarely a defining failure mode unless certain conditions apply.

According to the codes, no verification is needed if:

1 The edge distance in all directions is $c \geq 1.0c_{cr,sp}$ for single fasteners and $c \geq 1.2c_{cr,sp}$ for groups of fasteners and the member depth is $h \geq h_{min}$ in both cases, with h_{min} corresponding to $c_{cr,sp}$. Where the characteristic edge distance in the case of splitting under load, $c_{cr,sp}$, is found in the relevant European Technical Product Specification.

2 The characteristic resistances for concrete cone failure and pull-out failure (headed and post-installed mechanical fasteners) or combined pull-out and concrete failure (bonded fasteners) are calculated for cracked concrete. In addition,the reinforcement must resist the splitting forces and crack width should be limited to $w_k \leq 0.3mm$.

If neither of the two requirements are fulfilled, the characteristic concrete splitting resistance of a fastener, or a group of fasteners, shall be calculated according to equation 3.11.

$$N_{Rk,sp} = N^0_{Rk,sp} \cdot \frac{A_{c,N}}{A^0_{c,N}} \cdot \Psi_{s,N} \cdot \Psi_{re,N} \cdot \Psi_{ec,N} \cdot \Psi_{h,sp} \qquad [N] \tag{3.11}$$

where

$N^0_{Rk,sp}$ is given in the relevant European Technical Product Specification

$A_{c,N}, A^0_{c,N}, \Psi_{s,N}, \Psi_{re,N}, \Psi_{ec,N}$ according to for concrete cone failure where $c_{cr,N}$ and $s_{cr,N}$ shall be replaced by $c_{cr,sp}$ and $s_{cr,sp}$ respectively, which are taken as the minimum member thickness h_{min}.

and

$$\Psi_{h,sp} = (\frac{h}{h_{min}})^(\frac{2}{3}) \leq max\{1; (\frac{h_{ef} + 1.5c_1}{h_{min}})^(\frac{2}{3})\} \leq 2 \qquad [N] \tag{3.12}$$

3.1.5 Concrete blow-out failure

Concrete blow-out failure is relevant for fasteners placed close to a free end. Verification is needed if the edge distance $c \leq 0.5h_{ef}$. The characteristic resistance is calculated according to equation 3.13:

$$N_{Rk,cb} = N^0_{Rk,cb} \cdot \frac{A_{c,Nb}}{A^0_{c,Nb}} \cdot \Psi_{s,Nb} \cdot \Psi_{g,Nb} \cdot \Psi_{ec,Nb} \qquad [N] \tag{3.13}$$

For groups of fasteners perpendicular to the edge, verification is only required for the fasteners closest to the edge.

The characteristic resistance of a single fastener, not influenced by adjacent fasteners or further edges is obtained as given by 3.14.

$$N^0_{Rk,cb} = k_5 \cdot c_1 \cdot \sqrt{A_h} \cdot \sqrt{f_{ck}} \qquad [N] \tag{3.14}$$

where

k_5 = 8.7 for cracked concrete

= 12.2 for uncracked concrete

A_h as defined by equation 3.10.

3.2 Fédération internationale du béton

An alternative approach to the structural Eurocodes is the model codes found in Fib, which are presented in the following section. Due to a high degree of similarities between the two codes. Only differences and modifications to the Eurocodes are shown. The failure modes designed for are:

1 Steel failure

2 Pullout failure

3 Concrete cone failure

4 Splitting failure

3.2.1 Steel failure

Characteristic resistance $N_{Rk,s}$ of an anchor in case of steel failure is calculated according to equation 3.15.

$$N_{Rk,s} = A_s \cdot f_{uk} \tag{3.15}$$

where A_s is the anchorbolt tensile stress area and f_{uk} characteristic steel ultimate tensile strength. As can be seen when compared to same equation in Eurocode (see equation 3.1) it is identical with the exception that fib doesn't include a reduction factor of 0.9. Thus, the calculations in fib yields a slightly higher capacity for steel failure.

3.2.2 Concrete cone failure

Concerning concrete cone failure, the model codes according to Fib presents identical design procedures and equations as in the eurocodes. They do, however, differ when it comes to the factor k_1 which is 7.7 for cracked concrete and 11.0 for uncracked concrete compared to 8.9 respectively 12.7 for eurocode.

3.2.3 Pullout failure

According to fib bulletin 58 no reliable design models for calculation of the characteristic resistance for pullout failure are available. It is instead determined from the result of Approval tests.

3.2.4 Splitting failure

Just as in the Eurocodes, fib design the connections for anchor installation as well as for anchor loading. Failure during installation is avoided by following edge distances according to relevant Approval or evaluated based on the results from appropriate tests in the prequalification procedure.

Splitting failure due to anchor loading is verified as for in the Eurocodes as described in section 3.1.4. If not fulfilled they are designed through the use of equation 3.11 with the relevant modifications of parameters for fib described earlier in this chapter.

4 Finite element model

The study was performed using the finite element analysis software ABAQUS CAE 2019, used for modeling and analysis of mechanical components and assemblies as well as visualizing the results of the finite element analysis. This section describes the relevant theory and solving process used in the analysis.

4.1 Fundamentals of the Finite Element Method

The Finite Element Method is a well used method used for describing physical phenomena in engineering mechanics too complex to solve using analytical methods. A finite element model is obtained by dividing the structure into a number of well-defined smaller parts, referred to as finite elements. The behaviour of the material is approximated over each element instead of trying to find an approximation holding true over the entire studied region. [10] A problem as such is defined as *discrete* whereas a problem using infinite number of elements indefinitly and is solved using mathematical expressions such as differential equations are called *continuous*. [11]

Many different methods of discretization of a continuum problem have been proposed with the goal of finding an approximation with a degree of error as small as possible. The error in an FE-model approaches the true solution when the number of elements increases.

4.2 Solvers in Abaqus

The software consists of different parts, used for different practical purposes. The one used for this study was the Abaqus CAE (Complete Abaqus Enviroment), which is a graphical interface for pre- and post-processing. In this enviroment, two different solvers are available depending on which structural analysis is being performed. The Abaqus implicit solver is the one mainly used by structural engineers in static analyses while Abaqus explicit solver is mainly used in dynamic circumstances where high velocities occurs. It is, however, possible and useful for static analyses to use the dynamic explicit solver in case of high convergence problems. This is extra prominent for quasi-static problems where severe non-linearity is expected. [7]

Because of the large deformations expected from the interaction between the steel bolt and concrete and the implementation of a inelastic material model, it was deemed appropriate to make use of the dynamic explicit solver. The Abaqus Explicit performs inexpensive and computationally efficient calculations using small time increments when solving the problem. The main reason for the explicit solver is that it is appropriate when convergency issues is an expected problem. It is also found to be the most

widely implemented method for similar problems.

4.2.1 Quasi-static analysis

Since the focus of this thesis is to study static loading conditions while using dynamic solvers, a concept of quasi-static analysis has been adopted. A dynamic system usually exhibit oscillations and other time-dependant effects as a result of the implementation of velocity to the system. A quasi-static system therefore tries to avoid these problems by simulating static loading conditions through very low loading rates. This is done by applying boundary conditions to the loading area and performing displacement controlled loading. When running the simulation, it is advantageous to control that the kinetic energy in the model does not increase to a significant amount as this would introduce significant inertial forces to the system.

4.3 Concrete material model

Abaqus provides three different constitutive models for the analysis of concrete at low confining pressures:

- Concrete smeared cracking
- Brittle cracking model
- Concrete damaged plasticity

These are primarily based on the theories of fracture mechanics, plasticity theory and damage theory, or a combination of these, as defined in chapter 2.2.4. One defining feature for all of them is the concept of reduced stiffness under cracking, defined as a softening behaviour. [7, 12] The Concrete damaged plasticity model was adopted for this study and the others will not be considered further.

4.3.1 Concrete Damaged Plasticity

Concrete Damaged Plasticity, or CDP, is a continuum, plasticity-based, damage model of concrete. The general assumption made is that failure in concrete occurs through compressive crushing and tensile cracking of the material. It is, as is usual for plasticity-based models in Abaqus, an incremental material theory in which the mechanical strain is divided into an elastic and a inelastic part. [13, 12]

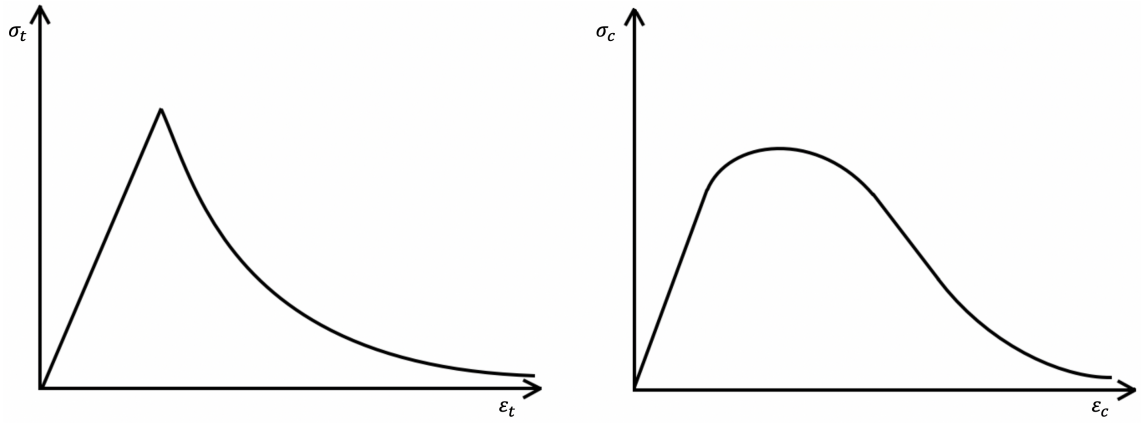

Figure 4.1: Response to uniaxal tension to the left and uniaxial compression to the right.

The response in the concrete to uniaxial tensile and compressive loading is described by a stress-strain diagram and is initially completely linear-elastic, as shown in figure 4.1 where left represents tension and right compression. Both curves describes a strain softening behaviour in the plastic part after failure stress is achieved, while the compressive curve also defines a prior stress hardening behaviour. Tensile strain softening corresponds to the propagation of micro-cracking in the material, initiated at failure stress levels. While the user defines the elastic modulus and the inelastic stress-strain data for the specific concrete specimen, it is assumed that it can be converted into stress-plastic strain data. This conversion is something that ABAQUS does by itself. [13]

When defining the postfailure tensile behaviour for the concrete damage plasticity model, tensile stiffening is required. It can be done using stress-strain relations where the postfailure stresses are defined as a function of the cracking strain. This is however mostly useful in a reinforced concrete element, while for a concrete member which is largely unreinforced it is generally accepted that the fracture energy cracking criterion developed by Hillerborg(1976) can be applied for practical purposes. [13]

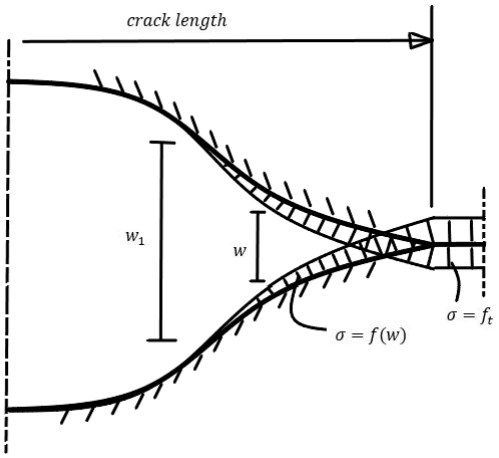

Figure 4.2: Reproduced illustration of stress distribution for cracks under tensile loads proposed by Hillerborg (1976). [14]

Hillerborg proposes a practical method to describe the stress-displacement relations for crack propagation. The crack is assumed to start propagating when the crack tip

reaches the tensile strength f_t and thereafter has a decreasing strength with increasing crack width w, instead of instantly being reduced to zero. The existence of stresses in a micro-cracked zone as in figure 4.2 has been found to be true if the corresponding displacement is small. The method uses a fracture energy parameter G_c to describe the amount of energy absorbed per unit crack area when the crack is widened from zero to or beyond w_l, found in figure 4.3. This stems from the fact that energy has been absorbed up to the initiation of the crack. The curve in figure 4.3 is chosen as to satisfy equation 4.1.

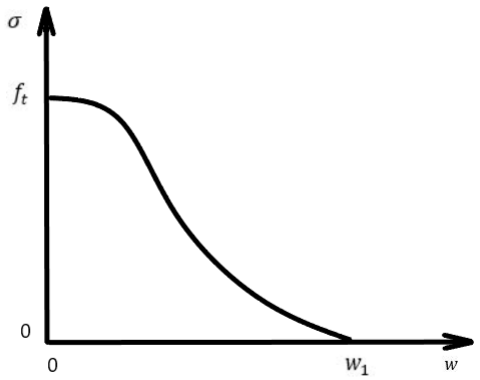

Figure 4.3: Reproduced illustration of theoretical stress-displacement relations for cracks under tensile loads proposed by Hillerborg (1976). [14]

$$G_c = \int_0^{w_l} \sigma dw \qquad [N/mm] \tag{4.1}$$

Different ways to implement this approach in an finite element analysis is discussed but a linear relation is proposed as a simple, continuous and suitable model. It also corresponds well to tension test results. This model is described in figure 4.4 as well as by formula 4.2. [14]

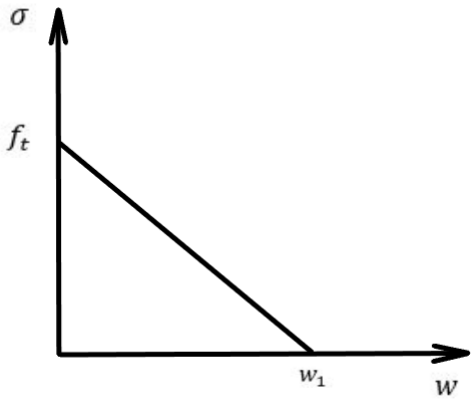

Figure 4.4: Reproduced illustration of practical stress-displacement relations for cracks under tensile loads proposed by Hillerborg (1976). [14]

$$w_l = 2G_c/f_t \qquad [mm] \tag{4.2}$$

When concrete is subjected to loading and especially cyclic loading, the concrete exhibits degrading elastic stiffness. This is taken into account in the Concrete Damaged Plasticity material model using two variables; d_t and d_c for tension and compression respectively. The variables are functions of plastic strain implemented in Abaqus in a tabular form as non-decreasing values between zero and one, as a function of the inelastic strain. The value represents the degree of damage where zero represents no damage and one represents maximum damage inflicted. The stress-strain relation under uniaxial loading is governed by equation 4.3 and 4.4, where E_0 is the undamaged elastic stiffness.

$$\sigma_t = (1 - d_t)E_0(\epsilon_t - {\epsilon_t}^{pl}) \qquad [MPa] \tag{4.3}$$

$$\sigma_c = (1 - d_c)E_0(\epsilon_c - {\epsilon_c}^{pl}) \qquad [MPa] \tag{4.4}$$

With the damage parameters, the elastic modulus and the associated inelastic strain given by the user, the plastic strain can be calculated using equation 4.5 to determine the occurring stresses.

$${\epsilon_c}^{pl} = {\epsilon_c}^{in} - \frac{d_c}{1 - d_c}\frac{\sigma_c}{E_0} \qquad [-] \tag{4.5}$$

Plastic tensile damage is available as input but not required considering the application is not essential. To describe the plastic strain in this case, the crack displacement have to be supplied and is then converted using a unit length. This will not be further explored since adding tensile damage parameters will not greatly benefit the models behaviour.

Multiaxial behaviour is generalised using the uniaxial behaviour together with the criterias and rules of the plasticity theory. These paramteres are determined using the following variables, defined by the user. Abaqus manual provides recommended values.

Dilation angle ψ is the dilation angle measured in the p-q plane. It is used to calculate the inclination of the plastic flow in high confining pressures. At low stresses it represents the internal friction of the concrete and decreases for increased strains and confining pressure. The minimum value of the angle is 0° and maximum value is 56.3°. Recommended value for design is somewhere between 30° and 40° but can vary largely based on loading scenarios and composition of concrete. [15][7]. In the CDP-model, an hyperbolic model is adopted and describes the yield surface for the model. It is useful for brittle materials where triaxial data for both compressive and tensile behaviour are available. While highly significant due to its deciding factor in the interaction between compressive and tensile behaviour, its value differ largely between applications. This is especially true for unreinforced concretes. [13] To accurately

describe the hardening and softening behavior of the concrete which greatly influences the results of this study, a parameter study will be conducted for the validation model in section 6.

Eccentricity $\in$ is the eccentricity of the plastic flow potential. The parameter defines at which rate the flow potential function approaches the asymptote for the hyperbolic mode. A value which tends to zero means that the flow fucntion tends to a straight line. In ABAQUS, the default value is 0.1 which indicates an almost constant dilation angle over a wide range of pressure stress values. [13]

$\mathbf{f_{b0}/f_{c0}}$ is the ratio of initial equibiaxial compressive yield stress to uniaxial compressive yield stress. For ABAQUS, the default value is 1.16 [13].

Ratio of the second stress invariant K_c on the tensile meridian to the compressive meridian for any given pressure variant at inital yield. The condition that it must satisfy is $0.5 < K_c < 1.0$ where the default value in ABAQUS is 2/3.

Viscosity parameter μ represents the relaxation time of the viscoplastic system. The default value is zero [13].

5 Calibration of FE-model

The adopted FE-model was calibrated by performing a parametric study. The aim was to achieve a correct failure load and behaviour of the model which would be applicable for the following analysis. The goal was to achieve a model which correctly replicates concrete cone failure of a bolted connection. This assumption of failure mode was found to be the most likely in the literature.

The following sections describe the model used and the result of the parametric study.

5.1 Experimental results of anchoring in concrete

The experimental tests chosen for this calibration were performed by Dr. Rasoul Nilforoush in 2017 as a part of his Doctoral thesis [8]. Six different test series were performed with varying material properties for the concrete and steel reinforcement. Focus of the experiment were partly on the load-carrying tensile capacity of cast-in-place anchors in order to get a better understanding of the fastenings and anchorage systems used in concrete.

For this calibration, test series (i) were chosen which consisted of Normal-Plain-Concrete (NPC) without any surface reinforcement. An experimental test without reinforcement was chosen to limit the scope of this thesis due to time shortages. Also, a focus of interaction between concrete and anchorage would be redirected to a study of the inclusion of reinforcement which is not the aim for this thesis. It has previously been the subject of a master thesis conducted at Chalmers University among others [16].

The test sample used in this calibration process consists of a M24 bolt with an anchor head diameter of 55 mm with a head depth of 30 mm and the effective embedment depth of the bolt is 220 mm. The size of the bolt was chosen in order to minimize the risk of steel failure occurring. The concrete slab is square with a length and width of 1 300 mm while the depth for the chosen test specimen is 660 mm. The concrete class that was utilised was C30/37. To permit an unrestricted concrete cone failure, a ring acting as steel support was added with the diameter of $d = 4.0h_{ef}$. A drawing of the test specimen is shown in figure 5.1.

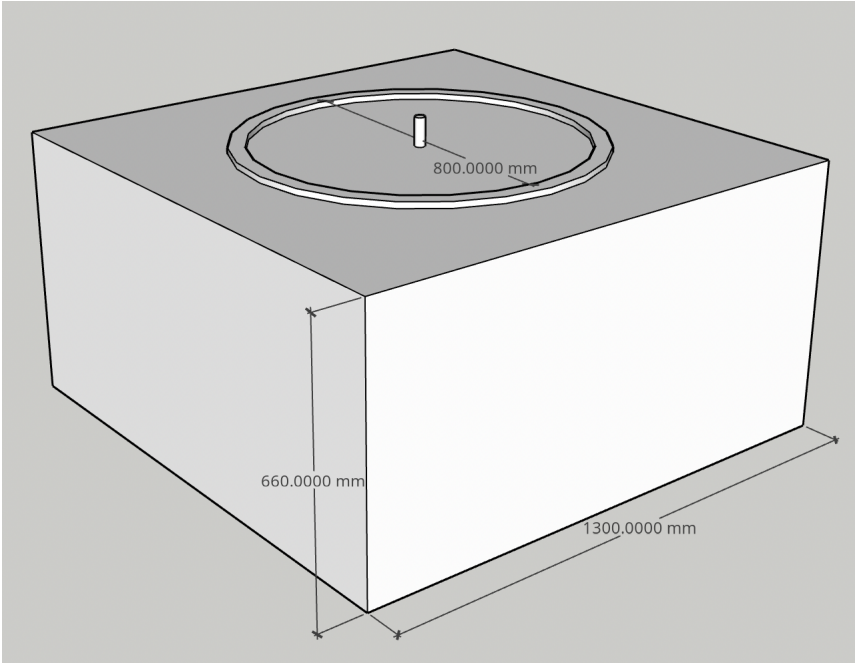

Figure 5.1: Reproduced illustration of test specimen used by Dr. Rasoul Nilforoush [8]

5.2 ABAQUS model

As previously described, the ABAQUS model is solved through the explicit solver. Due to its square shape, a quarter of the specimen can be modeled in order to reduce the size of the 3D model. Logically, the reduction of model size significantly reduces the computational time while still maintaining the behaviour due to boundary conditions which will be described in forthcoming section. The model used for calibrating the material behaviour is shown in figure 5.2.

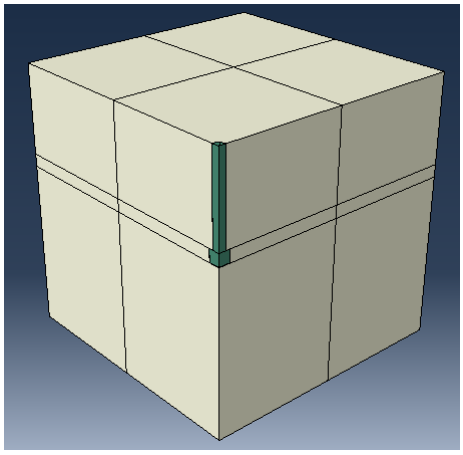

Figure 5.2: Quarter-sized model used for calibrating the material model.

5.2.1 Boundary conditions

In order to capture the behaviour correctly, while still maintaining a quarter of the size, symmetric boundary conditions are applied along the two center planes. The whole bottom surface of the concrete block is assumed to be fixed. The circular support along the concrete top surface is simplified to be applied on the circumference of the two outer edges in order to make the model as simple as possible without significantly affecting the end results. A simple view of the boundary conditions is shown in figure 5.3 and 5.4.

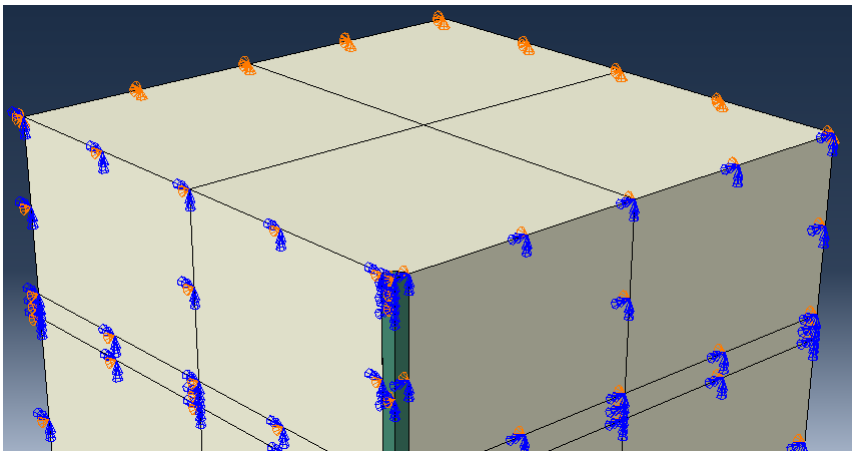

Figure 5.3: Boundary conditions applied to the model, bottom concrete plane is fixed.

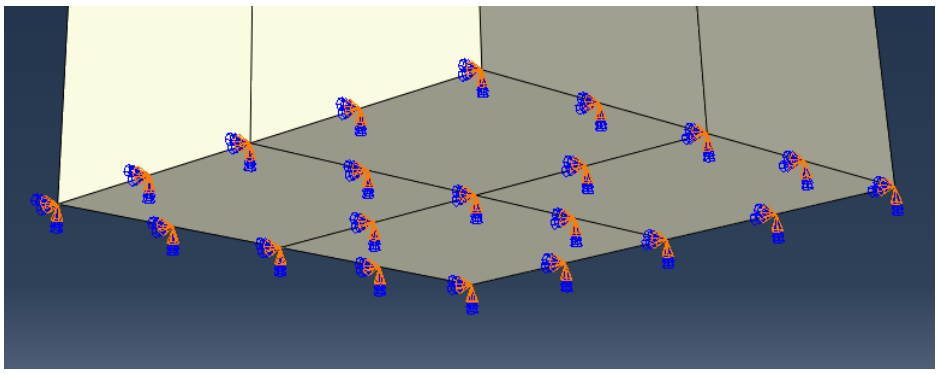

Figure 5.4: Pinned boundary condition on bottom concrete plane.

5.2.2 Contact properties

ABAQUS offers different options when defining contact properties between different materials in a model. For this thesis, the interaction between anchor head and concrete has been defined as *hard* in the normal direction. This means that the two materials can't penetrate each other once contact has occurred. In the tangential direction a frictionless behaviour has been adopted which can be seen as a conservative choice since there is friction between the anchor shank and concrete in reality. However, it is hard to estimate this friction coefficient and since the majority of the load is transferred through the mechanical interlock the simplification is deemed justified.

Also, to prevent direct contact between bottom of anchor head and the concrete, which can cause problems when running the simulation, a gap of 1 mm has been defined in this section.

5.2.3 Element type and mesh

The element type used in the model is a 8-node cubic element with reduced integration, called C3D8R. This means that one integration point is used, which simplifies computation and reduces the total time of the calculation. The element size chosen for the model was 20 mm on both the bolt and the concrete block. Previously research on similar models conducted at, among others, KTH concluded that 20 mm was the appropriate size when balancing correct material behaviour and computational time [17]. The meshed model is shown in figure 5.5

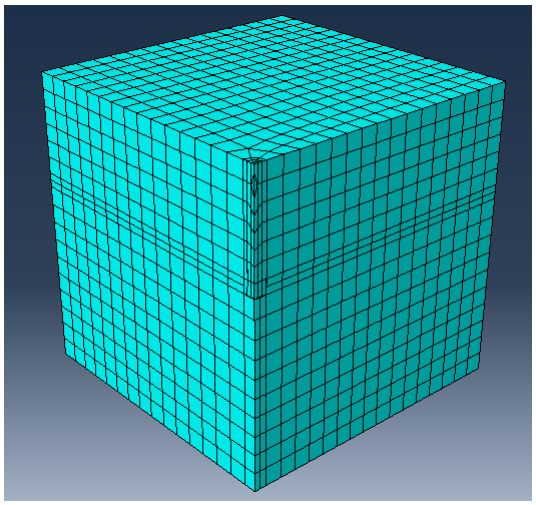

Figure 5.5: Meshed calibration model

5.2.4 Material properties

Material parameters are shown in table 5.1 and for the concrete properties the values are obtained from the tests performed by Dr. Rasoul Nilforoush [8]. Material strength for bolt class 8.8 were obtained from table 3.1 in Eurocode 93-1-8, section 3.1.1 [18]. To obtain correct concrete behaviour in ABAQUS, the concrete compressive strength is converted from cube strength to cylinder strength. The cube strength values are obtained from the tests perfomed at LTU where the strength was tested on concrete cubes while ABAQUS uses the concrete cylinder strength. The compressive cylinder strength is determined as 85% of the cube strength $f_{c,cu} = 0.85 \cdot f_{c,cy}$.

Table 5.1: Material parameters

Young's modulus - Concrete	E_{cm}	26.9	GPa
Young's modulus - Steel	E_s	210	GPa
Density - Concrete	ρ_c	2300	Kg/m^3
Density - Steel	ρ_s	7850	Kg/m^3
Poisson's ratio - Concrete	v_c	0.20	-
Poisson's ratio - Steel	v_s	0.28	-
Yield strength - Steel	f_{yb}	640	MPa
Ultimate tensile strength - Steel	f_{ub}	800	MPa
Cube compressive strength - Concrete	$f_{c,cu}$	40	MPa
Cylinder compressive strength - Concrete	$f_{c,cy}$	34	MPa

5.2.5 Compressive behaviour

The compressive behaviour of the concrete needs to be defined in ABAQUS which for this model is done as a tabular function. The input data is calculated according to section 3.1.5 in Eurocode 1992-1-1 [19] regarding the non-linear stress-strain relationship for concrete. Equation 5.1 describes the relation between the compressive concrete stress σ_c and strain ε_c.

$$\sigma_c = \frac{k\eta - \eta^2}{1 + (k-2)\eta} \cdot f_{cc} \tag{5.1}$$

where

η $= \varepsilon_c / \varepsilon_{c1}$

ε_{c1} is the strain at peak stress for a given concrete quality according to table 3.1 in Eurocode 2. For C30/37, the peak stress is 2.2 ‰ [19].

k $= 1.05 \cdot E_{cm} \cdot |\varepsilon_{c1}| / f_{cc}$

By using equation 5.1 the compressive stresses that will be added in ABAQUS are obtained. The corresponding inelastic strain is determined as the difference between the total strain and corresponding elastic strain according to equation 5.2.

$$\tilde{\varepsilon}^c_{in} = \varepsilon_c - \varepsilon^c_{el} \tag{5.2}$$

where the elastic strain is determined from Hooke's law $\varepsilon^c_{el} = \sigma_c / E_o$.

With the stress and corresponding strain determined, the compressive behaviour in figure 5.6 is obatined and the the values can be inserted as a tabular function in ABAQUS.

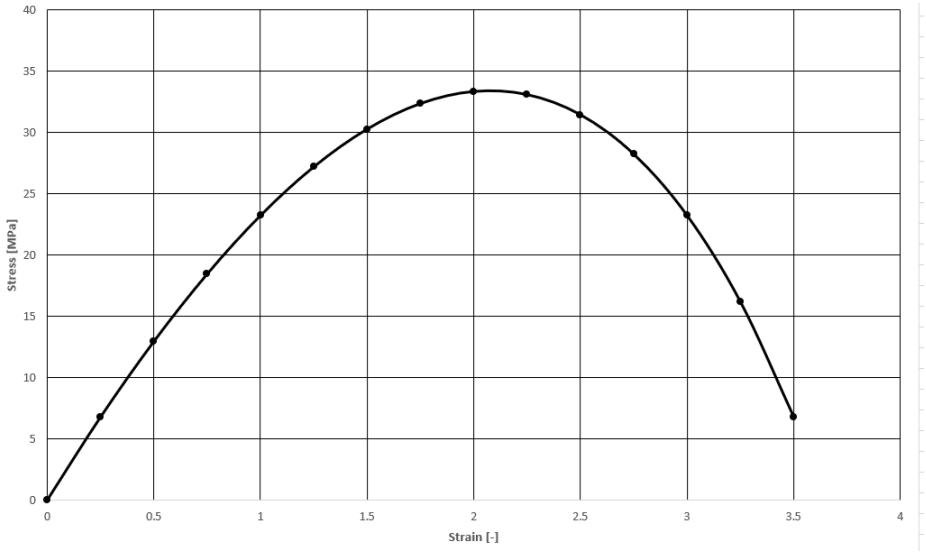

Figure 5.6: Compressive stress-strain behaviour for C30/37 used in tests.

5.2.6 Tensile behaviour

The tensile softening behaviour is determined in ABAQUS through the tensile strength of concrete and fracture energy. By adding this data to the program as a tabular function, it automatically adopts a linear description of the tension softening behaviour where the area under the graph is the prescribed fracture energy and maximum value is the tensile strength. For this model, the values are obtained from mean values measured by Dr. Nilfouroush [8] and presented in table 5.2.

Table 5.2: Prescribed values for tensile softening behaviour of concrete

Tensile strength	f_{ctm}	3.2	MPa
Fracture energy	G_f	147	N/mm

5.2.7 Defining loads

For the experimental tests used as calibration in this study, the load was applied on the bolt with a loading rate of 1 mm/min. To achieve the correct behaviour in both materials the load is applied as an displacement on the top surface of the anchor bolt. In addition to resembling the actual loading situation from the test, the reason for this is that the computational time is shorter for prescribed displacement due to the nature of the program which is based on the FE-formula $F = k \cdot d$ [20]. Displacement controlled loading also captures the softening curve of the concrete better which is not possible with force controlled loading. Thus, the load is applied as a displacement of 15 mm over a longer time span in order to avoid dynamic effects and a stiffer material behaviour than expected. By minimizing the dynamic effects a quasi-static analysis is also achieved due to the slow velocity of the load.

5.3 Results

A parametric study on the dilation angle was performed to make sure that the model used in later analysis was able to accurately describe the behaviour of concrete cone failure. Four simulations with different dilation angles were carried through and the result is found in figure 5.7.

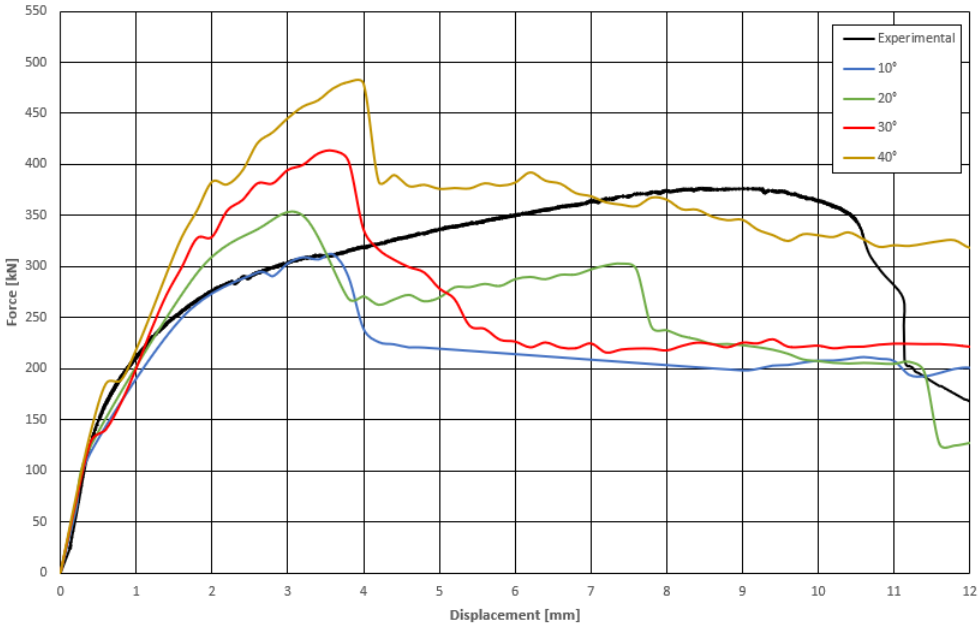

Figure 5.7: Force-displacement diagram for the experimental test conducted by Nilforoush.

As can be seen from the graph above, they all capture the behaviour of the concrete very well. However, high values on the dilation angle overestimate the failure load. This can, for example, be seen for a dilation angle of 40° where the failure load is above 500 kN. The failure load decreases with lower dilation angle and as can be seen from figure 5.7 a dilation angle of 20° has the best agreement with the experimental failure load.

Considering the experimental tests the model is based on was performed in such a way that concrete cone failure was achieved, it was important to verify that such was the case for this model as well. Concrete cone failure is the expected failure mode in the analysis in chapter 6 and the only failure mode verified against. The stress distribution shown in figure 5.8 depict a behaviour consistent with such of a concrete cone failure.

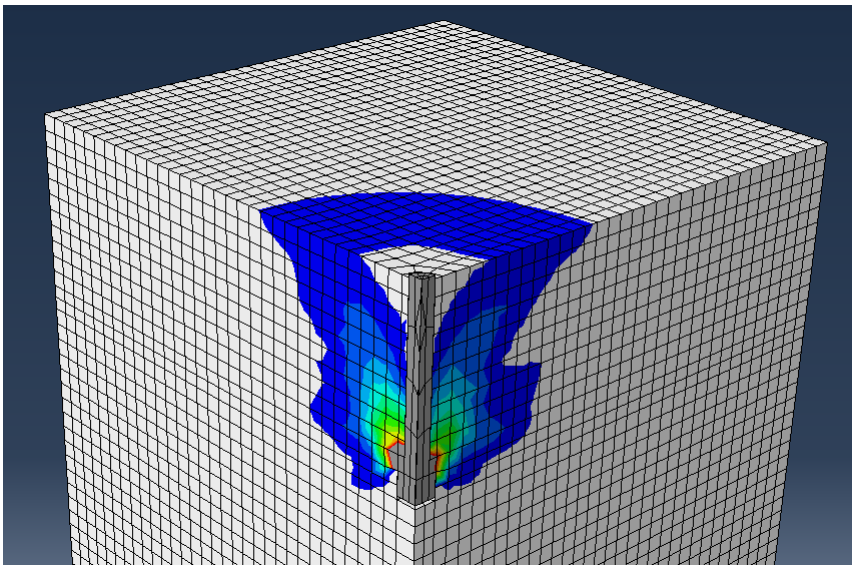

Figure 5.8: Concrete cone breakout failure mode seen just before the concrete fractures. Image is taken from the test with 10° dilation angle.

As can be observed when comparing experimental values and finite element analysis, the experimental result shows a more ductile behaviour. The displacement at failure load for the finite element analysis is around 50 % of the displacement for the experimental test. There are numerous factors that can contribute to this difference in behaviour. To begin with, the steel material is deemed as more brittle in the model compared to reality which lead to smaller displacement. The definition of contact properties could also affect the behaviour since it is assumed to be frictionless in the normal direction. This means that there is no resistance due to friction between the anchor shaft and concrete. For section 6, a dilation angle of 20° will be used for all analyses.

6 Finite element analysis of steel-to-concrete joint

This chapter presents the analysis and results of the finite element tests of the two evaluated joints, the standard design and the narrow design. Each model was subjected to multiple load cases in a static analysis and resulting failure mode compared with the relevant design codes. The purpose was to investigate the possible difference in failure modes or distribution of loads between the designs.

6.1 Design simplifications

In case of space deficiency, it is common to deviate from the design code requirements when designing a joint. In the specific case being examined, the corner geometry of the plate was forced to deviate from the optimal design case because of set prerequisites. The concrete foundation of this elevator shaft creates an asymmetric plate to allow for the movement of elevators. The designers choice to increase the bolts and relocate them without changing the dimensions or strength class is assumed as a conservative design choice. The dimensions for the two connections is presented in figure 6.1.

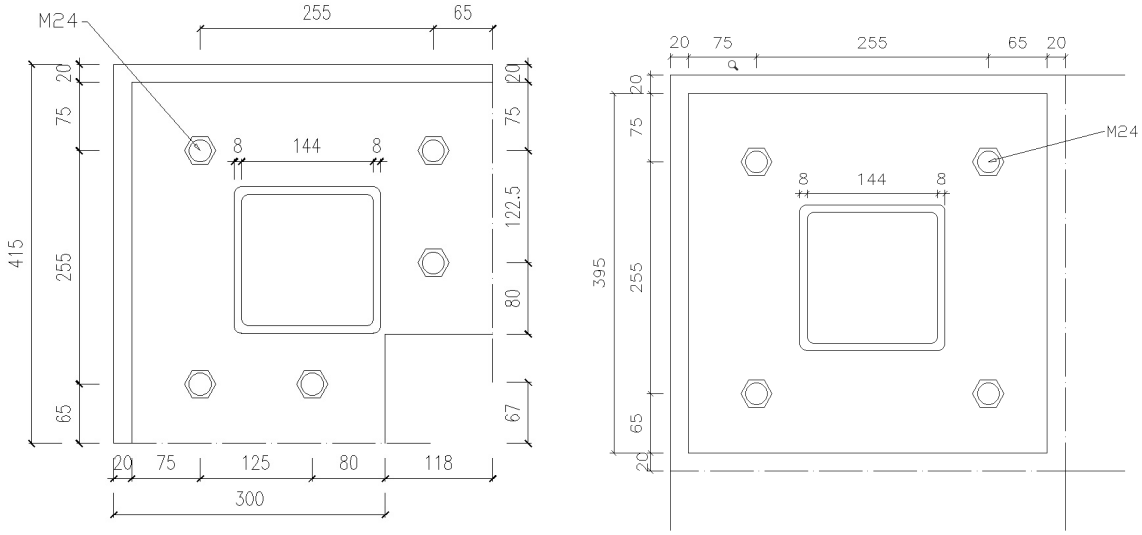

(a) Alternate connection due to narrow corner **(b)** Standard connection

Figure 6.1: Geometric properties of the two studied connections.

The connection consists of a 395x395 mm^2 steel plate joining the concrete to a Hot Formed Rectangular Hollow Section column (HFRHS) with outside dimensions of 160x160 mm^2 as can be seen in the figure above. Expanding grouting is used between the plate and concrete in both connections to achieve full contact and avoid buckling in the fastening bolts. The bolts are produced in with a diameter of 24 mm and are placed according to minimum edge distances. For the proposed connection, they are however asymmetrical as a result of the non-symmetrical design. The plate thickness is 30 mm.

6.2 Material model

The material model used was validated and calibrated in accordance with chapter 5. Parametric studies performed during that stage lays the basis for the material parameters chosen for the full analysis.

Concrete compressive strength is described through tabulated values according to figure 5.6 in section 5.2.5 and the tensile softening is described using a linear regression with a tabulated fracture energy of 145 N/mm^2. Damage parameters have been tabulated using formulas found in chapter 4.3.1 and plotted against the inelastic strain. The steel parts are modelled as elastic-perfect plastic. Is is assumed that the plate is of steel grade S355 with a thickness of 30 mm where relevant data is obtained from table 2.1 in *Regel-och formelsamling* [3]. All relevant data for the steel connections can be found in table 6.1 and 6.2.

Table 6.1: Material parameters of steel plate.

Young's modulus	E_s	210	GPa
Density	ρ_s	7850	Kg/m^3
Poisson's ratio	v_s	0.28	-
Yield strength	f_y	345	MPa
Ultimate strength	f_u	470	MPa

Table 6.2: Material parameters of steel bolts.

Young's modulus	E_s	210	GPa
Poisson's ratio	v_s	0.28	-
Yield strength	f_{yb}	640	MPa
Ultimate tensile strength	f_{ub}	800	MPa
Density	ρ_s	7850	Kg/m^3

6.3 Finite element model

Both models were built using the same C3D8R hexagonal finite element used previously with a mesh size of 20 mm. The analysis carried out was, as in chapter 6, quasi-static with high expected non-linearity, making a dynamic explicit solver the best option to avoid convergence problems. The step time for the analyses conducted in the forthcoming sections was 50 seconds, which yielded a computational time of around 16-20 hours per simulation. This was chosen since the dynamics effects were deemed negligible while also maintaining a reasonable time of simulation. To reduce the complexity of the model, the only part of the HFRHS column that is modeled is the connecting area onto the steel plate. By measuring from the centre-to-centre of the column this yields a loading area of 152x152 mm^2.

6.3.1 Boundary conditions

To be able to study the connection when subjected to different loads, a part of the structure was isolated. The models where given an elongation of the concrete of 700 mm i both directions from the end of the steel plate. The section cuts was given fixed boundary conditions over the surface, just as for the bottom surface. The length was determined to be enough to achieve minimum impact on the results from the edges of the model. Boundary conditions applied on the standard model is shown in figure 6.2. It should be noted that the boundary conditions are identical for the two models.

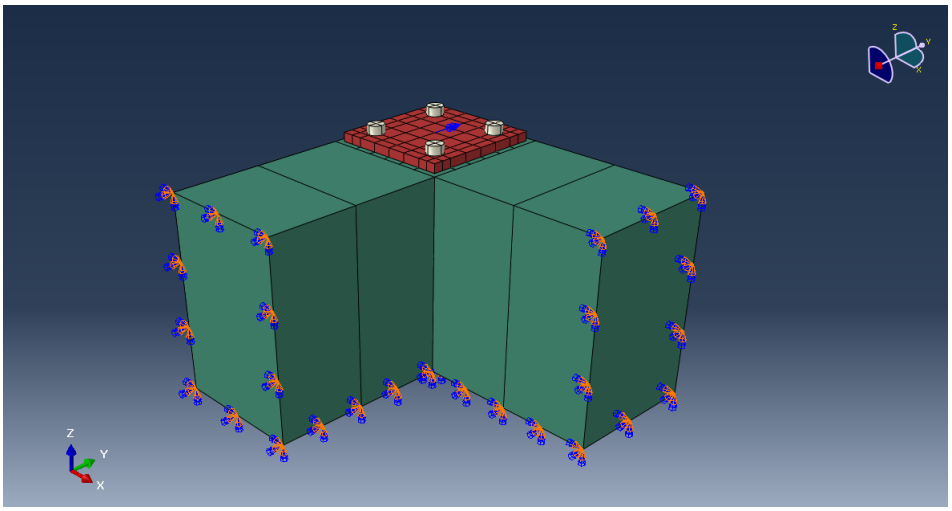

Figure 6.2: Fixed boundary conditions on sides and bottom of the standard model (applied on both models).

6.4 Analysis procedure and loads

The tests performed aimed at getting a better understanding of the behaviour of the narrow design and its mode of failure compared to the standard connection. Two general analyses have been performed based on the two simple static load cases: pure tension and a moment around the x-and y-axis.

6.4.1 Tensile analysis

Tensile displacement controlled loading of the entire component was performed for both models. The displacement was configured to simulate the tension resulting from the welded column during uplift. The force was assumed to work constantly over an area equal to the size of the base of the column. The applied displacement had a magnitude of 5 mm, after which no more failure could be seen. Displacement of 5 mm instead of 15 mm were used since failure occured at around 6 mm for the validation model and it was deemed that the failure would occur earlier for the connections due to the more brittle behaviour from the anchor group. An illustration of how the displacement was applied together with the loading area is observed in figure 6.3.

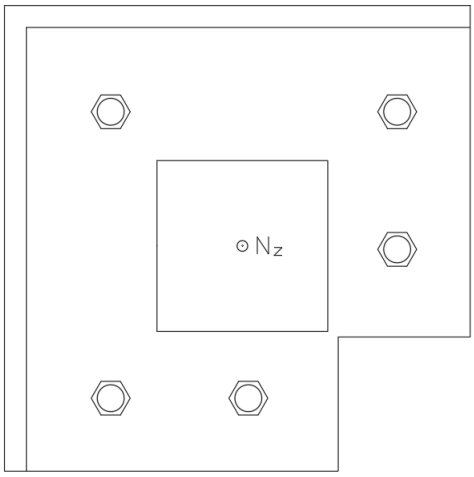

Figure 6.3: Illustration of how the displacement controlled tensile analysis was performed.

Expected results are predicted to show the maximum tensile force in the group of bolts which, in comparison with relevant design codes, could be used to predict the failure mode of the connection. Therefore, the data of the sectional forces in the most loaded surface was requested from the software.

6.4.2 Moment analysis

Analysis of moment capacity was also conducted for both models through rotational displacement. The rotational displacement was applied along the x-axis and y-axis according to figure 6.4 in both directions where the positive directions is presented in the figure. For each simulation only one moment in one direction was applied, resulting

in total of four simulations conducted. The size of the rotational displacement was 0.05 radians based on earlier conducted simulations on similar models.

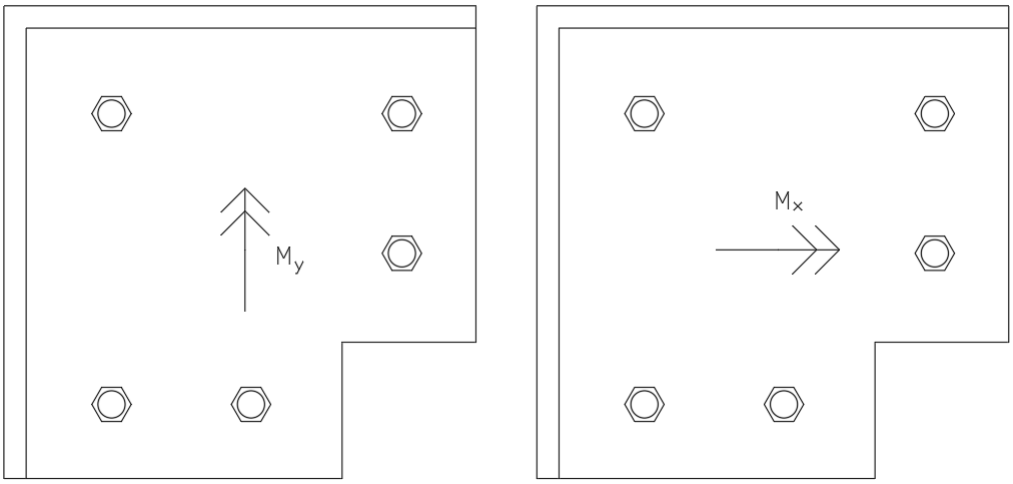

Figure 6.4: Illustration of how M_y and M_x were applied on the narrow connection. Same directions applies to the standard one. In the figure positive direction of the moments is shown

6.5 Analysis of standard connection

6.5.1 Load capacity according to design code requirements

Load capacity of the standard design was determined using both design guides presented in chapter 3, SS-EN 1992-4:2018 and fib Bulletin 58. Equation 3.2 from section 3.1.2 were used. Two calculations were carried out for each design code, one with the concrete edges included and one ideal case where it is assumed that there is no concrete edges nearby. Design loads are presented for the three main expected failure modes for a group of anchors; steel failure, pullout failure and concrete cone failure. These are later compared with the results of the finite element analysis. Failure in the plate is not considered in this analysis.

Results of the calculations is shown in table 6.3 and 6.4 and presents the decisive load value for concrete cone failure on a group of fasternes. Further information on the proceedings of the calculations can be found in Appendix B.

Table 6.3: Concrete cone failure capacities according to design codes.

Load case	SS-EN 1992-4	fib
Tensile load [kN]	228	198
Positive moment [kN]	197	171
Negative moment [kN]	315	273

Table 6.4: Other relevant capacities according to design codes.

Mode	SS-EN 1992-4	fib
Steel failure for a fastener [kN]	326	362
Pull-out failure for a fastener [kN]	810	-

6.5.2 Results of tensile analysis

The results of the standard model are presented through force-displacement graphs and these can be compared to design capacities according to codes. In addition, the load distribution on each individual anchor is also presented. The reader should take note that most of the graphs in this, and forthcoming sections, have been processed and smoothed out in order to be more similar to a quasi-static behaviour. This is done in order to remove small dynamic effects which are hard to avoid completely, no matter the velocity of the applied load. The results from the tensile analysis on the standard connection is presented in figure 6.5 together with load capacities according to the design code in table 6.3 and 6.4.

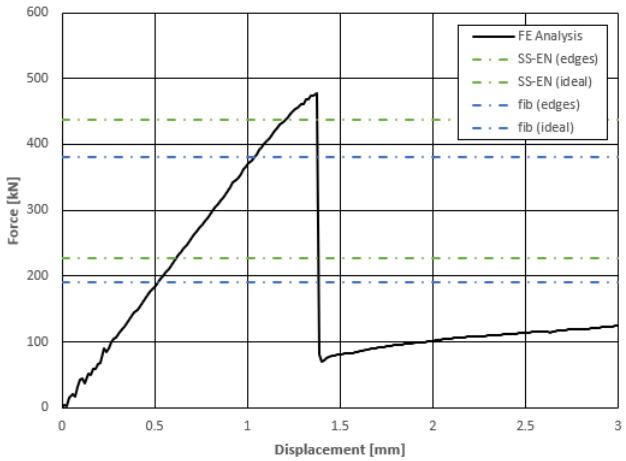

Figure 6.5: Force-displacement curve for the standard connection exposed to pure tensile load.

The model shows early signs of dynamic effects in form of oscillation, however minor and temporary, which is not considered to have significant impact on the overall result. A maximum load of 477 kN is reached before failure. The pre-failure behaviour seen in the graph shows a linear behaviour with small signs of plasticity. After failure a recovery at 70 kN is made, showing the existence of post-failure stiffness. The load distribution on the individual anchors is presented in figure 6.6.

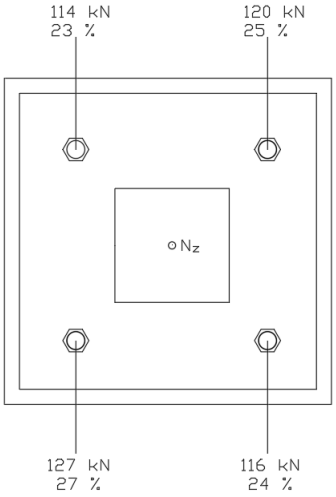

Figure 6.6: Distribution of the load on each anchor.

When comparing to the chracteristic design values according to Eurocode and Fib, as determined in section 6.5.1, with the maximum capacity of the model, also presented in figure 6.5, an overcapacity of 109% and 141% respectively is found when taking edge distances into account. When designing for an ideal scenario where edge distances does not influence the capacity an overcapacity of 8.9% and 25.5% is found compared to Eurocode and Fib.

As can be expected from the symmetrical design of the connection, the load is evenly distributed on all four anchors with almost 25 % distribution on each anchor. The small difference in distribution could be due to a number of reasons. It is suggested that the main factor is that the edge distance, in both vertical and horizontal direction, differs between all of the anchors and thus the load distribution will alter accordingly. When summarizing all individual normal forces in the anchors from figure 6.6, they show consistent force as for the data collected for the entire connection presented in figure 6.5.

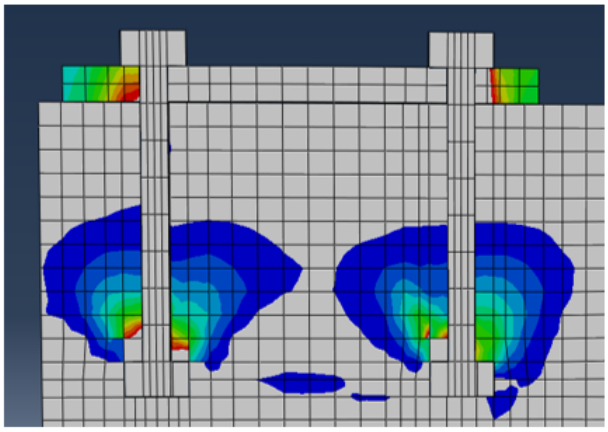

Figure 6.7: Stress distribution at failure for the standard model.

Figure 6.7 shows the build up of stresses in the group of anchors when subjected to displacement. The stress distribution at failure does not itself give conclusive evidence on which failure mode the connection is subjected to. It does however provide an

indication on which further analysis could based. The stress distribution in figure 6.7 does not exclusively coincide with that of a concrete cone failure found in literature. Some formation of angled stress concentrations are present as well as a large concentration of stresses right at the contact areas. This could suggest a combination of concrete cone failure and pull-through failure.

6.5.3 Results of moment analysis

The behaviour for the standard design when subjected to moment around x- and y-axis is presented in figures 6.8a and 6.8b respectively. The blue lines presents the results of positive moment as defined in section 7.4.2 while the red represent the negative. Evidently, significant differences in the values of peak load and shape of the loading curves occur. Small differences were anticipated due to the asymmetry of the force distributing steel plate as well as due to its location in the corner of a concrete foundation. However, the great differences in overall plastic behaviour was not expected.

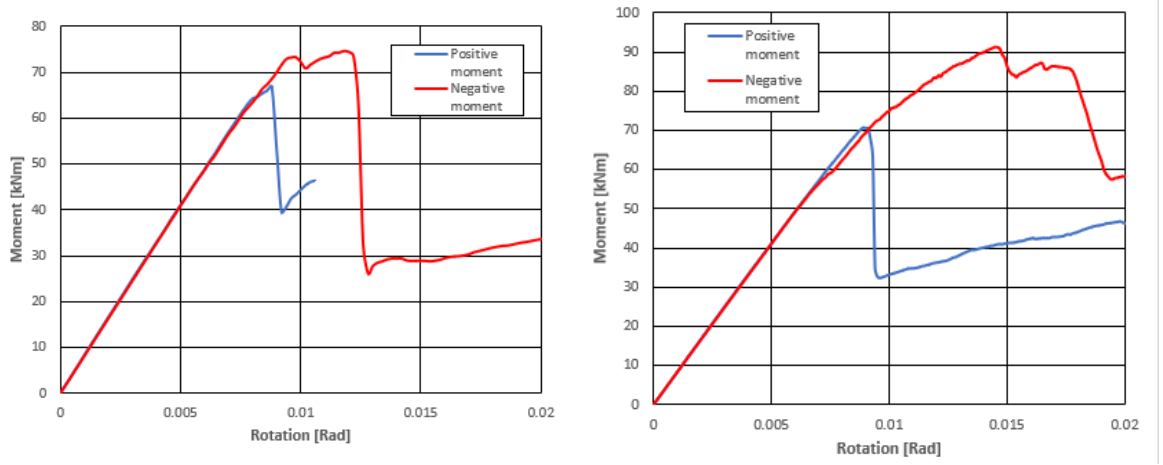

(a) Positive and negative moment along x-axis. **(b)** Positive and negative moment along y-axis.

Figure 6.8

Maximum loads for the positive moment around both axes (blue graph, figure 6.8) show a difference of 5.5% in favour of the y-axis with a maximum value of 71 kNm. They similarly reach failure at a rotation of 0.0088 and 0.0089 radians respectively. In contrast, when applying the load in the reversed direction (red graph, figure 6.8) a difference of 22.3% with a maximum load of 91 kNm is achieved. For both of the positive directions no plastic behaviour can be observed. Failure for the negative moment around the axis occurs at a rotation of 0.0118 radians while at a rotation of 0.0145 radians for the y-axis.

Post-failure recovery is prominent for all tests with a loss of between 35 and 63 pro cent without any prominent correlation. In the tests subjected to negative moments, a short dip in strength is seen. This recovery, could from examination of the sequence of events in the model, be determined to happen due to successive failure of the bolts in tension. After the first bolt has reached maximum capacity, redistribution of loads occur while the bolt that has failed starts to show plastic behaviour. This could explain

the plastic behaviour in between the two load peaks.

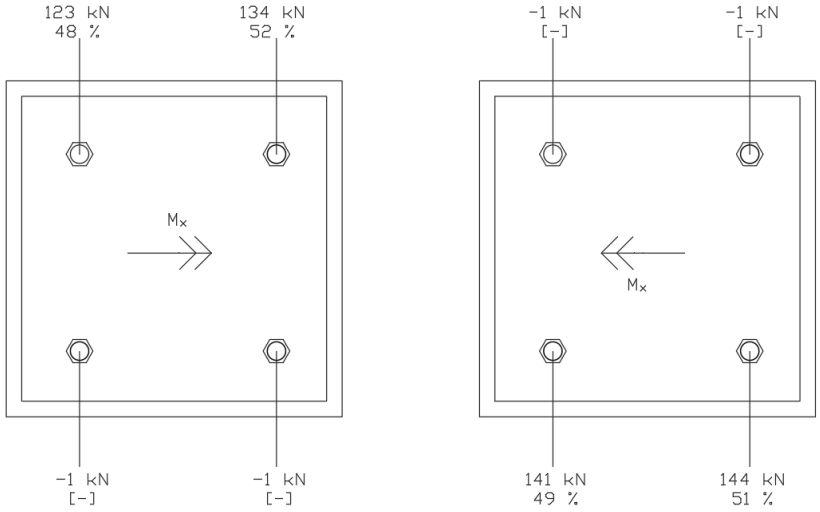

(a) Moment along x-axis (left positive, right negative direction.)

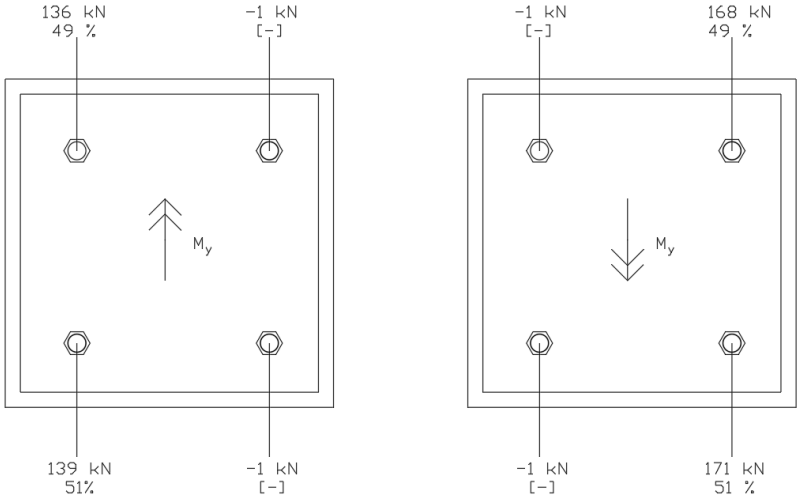

(b) Moment along y-axis (left positive, right negative direction.)

Figure 6.9: Load distribution on individual anchors for all moment directions. Positive values indicates anchor in tension, negative is in compression.

Figure 6.9 displays maximum normal force achieved in each bolt before failure for all the examined load cases. Relatively small differences in load distribution occurs, as expected because of the somewhat symmetrical geometry of the steel plate. Notably however, the bottom right bolt receives a higher concentration of forces and is the first to reach capacity when loaded with negative loads. For the two positive moments however, it is not the same bolt that takes up the maximum force.

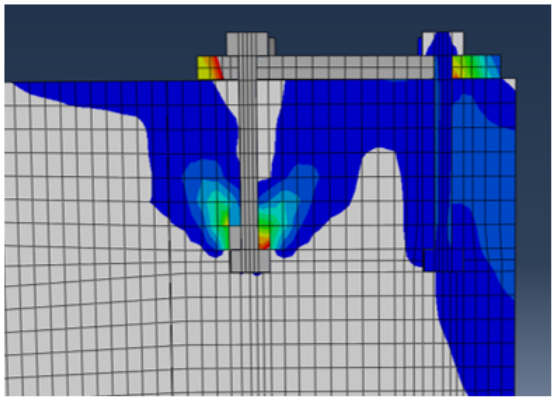

Figure 6.10: Distribution of stresses in the standard model at failure.

By examining the distribution of stresses in the concrete at maximum load, an understanding of the expected failure modes could be formed. In figure 6.10, which depicts the stress distribution of the standard model subjected to negative load around the y-axis, a build up of stresses could be seen at the contact between the head of the bolt in tension and concrete as well as a widespread presence of stresses in the compressed part of the concrete. The tensile stresses show a distribution in a direction angled approximately between 10 and 30 degrees away from the normal direction of the bolt. This coincides with the theoretical assumptions about the formulation of cracks for concrete cone failure modes. Since crack propagation was not included in this thesis' scope, a solid conclusion of the failure mode could not be formed just based of this result solely.

Table 6.5: Comparison of design and model capacities for concrete cone failure for a group of anchors in tension.

Load case	SS-EN 1992-4	fib	Model
M_x positive [kN]	197	171	257
M_x negative [kN]	315	273	285
M_y positive [kN]	179	171	275
M_y negative [kN]	315	273	339

Table 6.6: Comparison of other relevant capacities according to design codes and model capacities.

Mode	Pull-out EN	Steel fail EN	Steel fail fib	Model
M_x + [kN]	1620	652	724	257
M_x - [kN]	1620	652	724	285
M_y + [kN]	1620	652	724	275
M_y - [kN]	1620	652	724	339

As a secondary tool to understand the type of failure mode, comparison with relevant design codes was performed. In table 6.5 the design values for concrete cone failure for a group of fasteners in tension is compared to the sum of the models fasteners in tension, as seen in figure 6.9. In general, Eurocode proves to be less conservative than fib and in most cases seem to match the tested result relatively well. The results does, however, prove the conservative nature of both design codes.

Compared to the pure tensile case, the Eurocode exhibits an overcapacity. Considering the finite element analysis was conducted on a model with short edge distances this is regarded as a reasonable result. Compared to other relevant failure modes, as presented in 6.6, a much larger difference is observed. Interestingly the model provides a capacity higher than concrete cone failure which means that the expected failure mode could possibly be a combination of more than one mode. Considering the overcapacity pendulate between 30% and 50% it is, however, reasonable to assume concrete cone failure could be a decisive failure mode.

6.6 Analysis of narrow corner design

Analysis of the narrow design were conducted with identical load cases as for the standard design.

6.6.1 Results of tensile analysis

The results from the tensile analysis conducted for the narrow design is presented in figure 6.11.

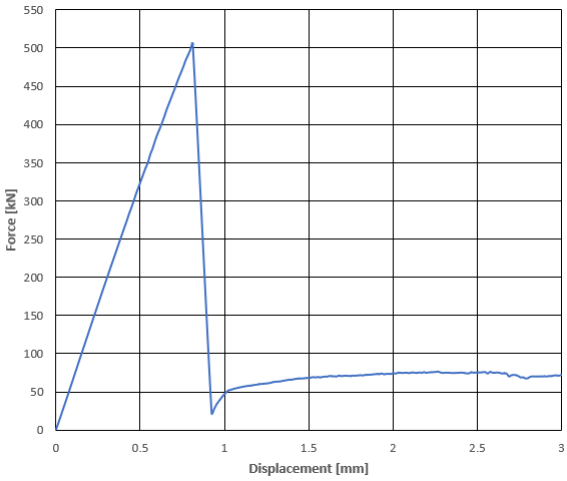

Figure 6.11: Force-displacement graph for the narrow corner design.

From the model it can be concluded that a load of 505 kN is reached before failure occurs. As for the standard design, the post-failure behaviour is linear with little plasticity. After failure, a recovery occurs at around 50 kN. Stress distrubtion in the concrete caused by the tensile load is presented in 6.12 and 6.13.

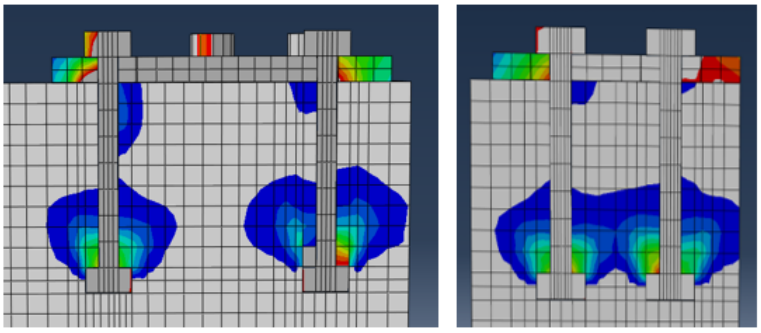

Figure 6.12: Stress distribution at failure for the narrow corner model closest bolts (left).

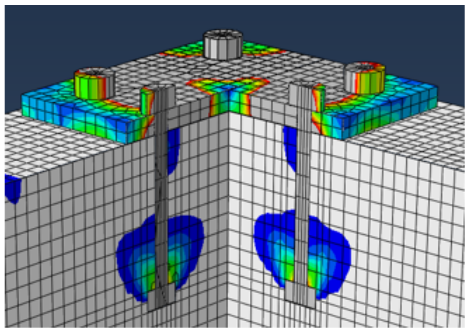

Figure 6.13: Stress distribution at failure for the narrow corner model bolts at steel plate cut-out.

The load distribution on each individual anchor is presented in figure 6.14. As one could expect, the distribution is not as equal as it were for the standard connection. It differs 20 kN between the largest and least loaded anchor for this design which in the end makes a different of around 6 %.

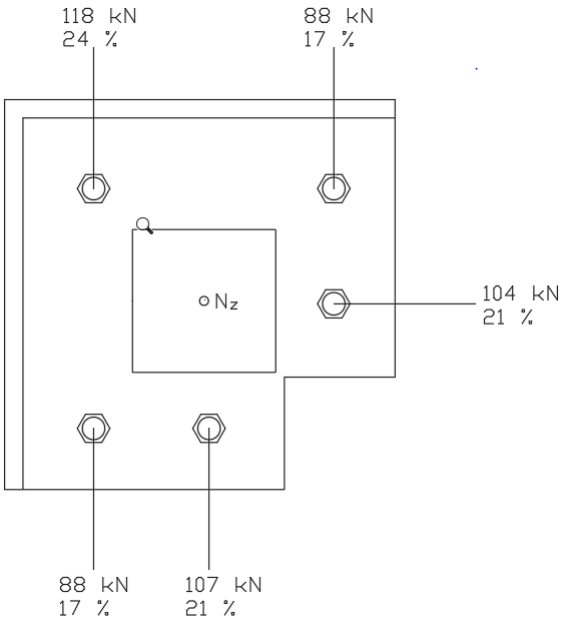

Figure 6.14: Distribution of the load on the anchors.

6.6.2 Results of moment analysis

The load case of positive and negative moment applied on the steel plate along x- and y-axis is presented in figure 6.15

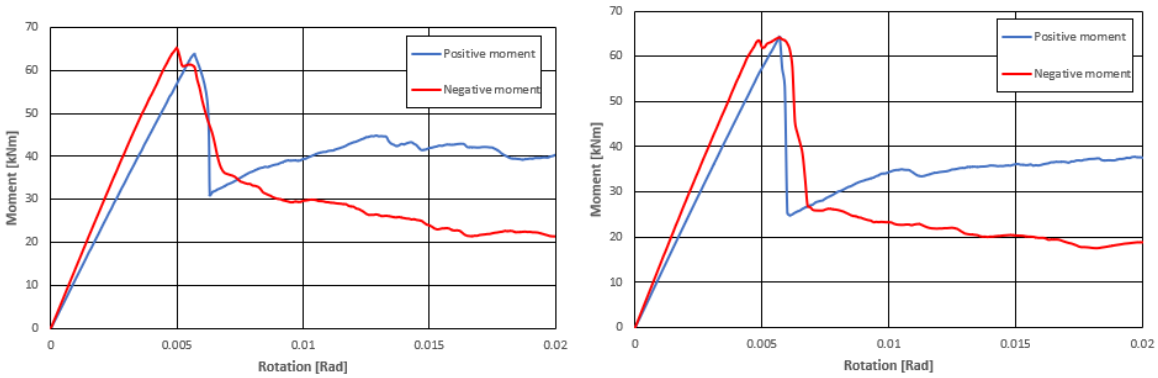

(a) Moment along x-axis

(b) Moment along y-xis.

Figure 6.15: Moment-rotation curves for the narrow corner connection.

The model predicts similar peak load along all four directions where failure is around 63 kNm, positive moment along x-axis (blue graph figure 6.15a) achieves highest peak load of 63 kNm. Pre-failure behaviour is brittle with little to no plasticity along all four directions as well. For the negative moment in both directions a small recover occurs shortly after failure. This is due to the anchors not failing all in once but rather failure of one and then a short recovery until the next one fails. The positive moment along both directions share a similar rotation at the point of failure of 0.006 rad and for the negative moment the rotation is same as well were the first anchor reaches failure at 0.005 rad and then the second anchor fails at around 0.0053.

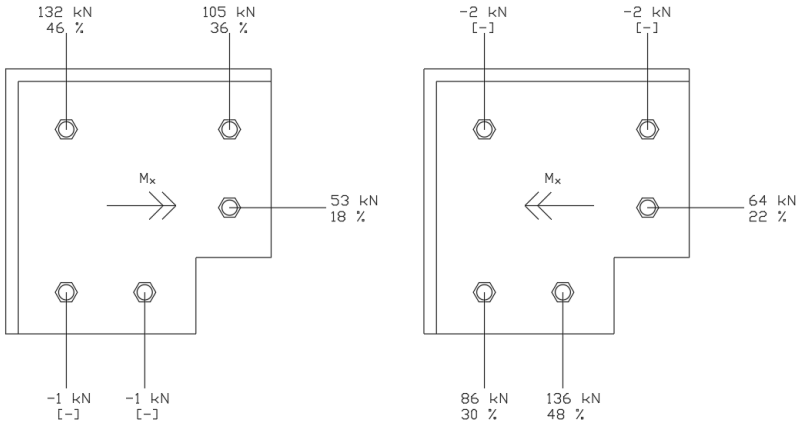

(a) Load distribution for Moment along x-axis (left positive, right negative).

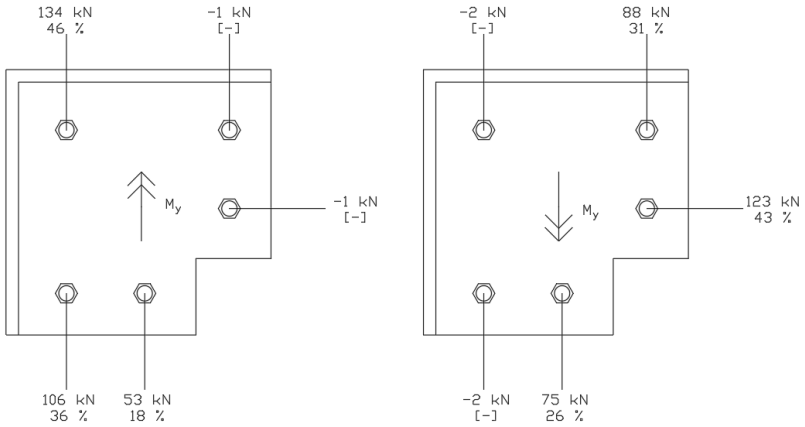

(b) Load distribution for moment along y-axis (left positive, right negative).

Figure 6.16: Load distribution on individual anchors for all moment directions. Positive values indicates anchor in tension, negative is in compression

Load distribution on the bolts for all load cases is presented in figure 6.16. By analysing the redistribution of the load an understanding of the pattern can be obtained. One anchor is exposed to the heaviest force of 123-136 kN where the largest one occurs for negative moment around y-axis (figure 6.16b right image). The anchor that is exposed to the highest force is in two occasions the anchor that is perpendicular to the angle of the applied rotation (see negative moment in figure 6.16a and 6.16b). In the other two cases it is the unsymmetrical geometry of the anchors exposed to tension that causes the load distribution. The bolt that are along the centre-line of the applied rotational displacement is endures the lowest force in the tensile area.

Stresses in the concrete at the point of failure at different anchors in the concrete is presented in figure 6.17 and 6.18.

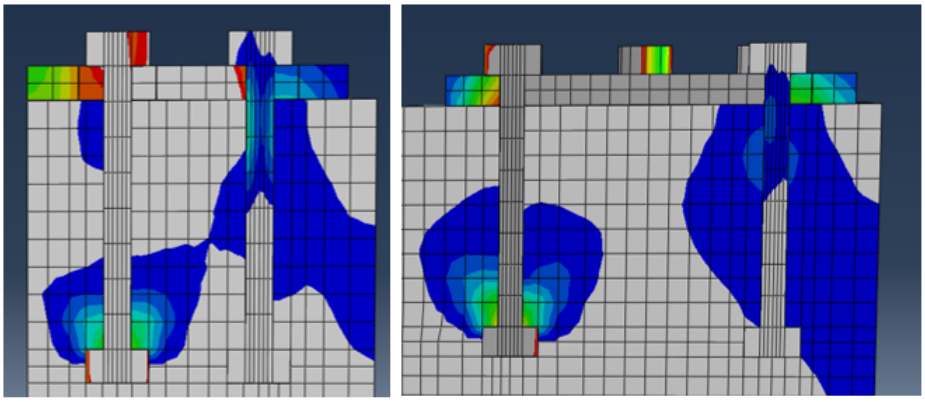

Figure 6.17: Stress distribution at failure for the narrow corner models closest bolts (left) and the ones furthest apart (right).

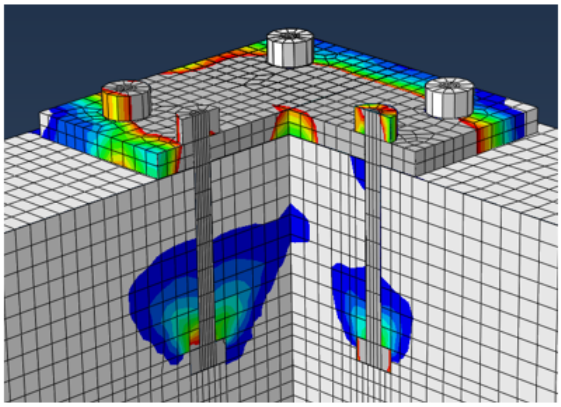

Figure 6.18: Stress distribution at failure for the narrow corner models bolts at steel plate cut-out.

Even though no solid conclusions can be drawn regarding the failure mode of the connection by just analyzing the stress concentrations presented in figure 6.17 and 6.18 as discussed in section 6.5.3, they could give an indication of the behaviour of the concrete at maximum load. The figures show a large concentration of tensile stresses above bolt heads loaded in tension. However, no clear indication of distribution corresponding to the expected concrete cone failure mode is present. Therefore it is reasonable to believe either a change of failure mode or a combination of failure mode is achieved. When comparing with literature on the subject and previous tests, it is clear that such a case is not unusual involving pull-through behaviour and concrete cone behaviour. The pull-through failure mode produce a more ductile failure with lower maximum loads due to the crushing of concrete at the contact area between bolt head and concrete.

6.7 Comparison and evaluation of results

To better understand the effect of examined simplification, comparison between the models results are made in this section and evaluated against expected results. The difference of the two models in tensile loading is presented in figure 6.19.

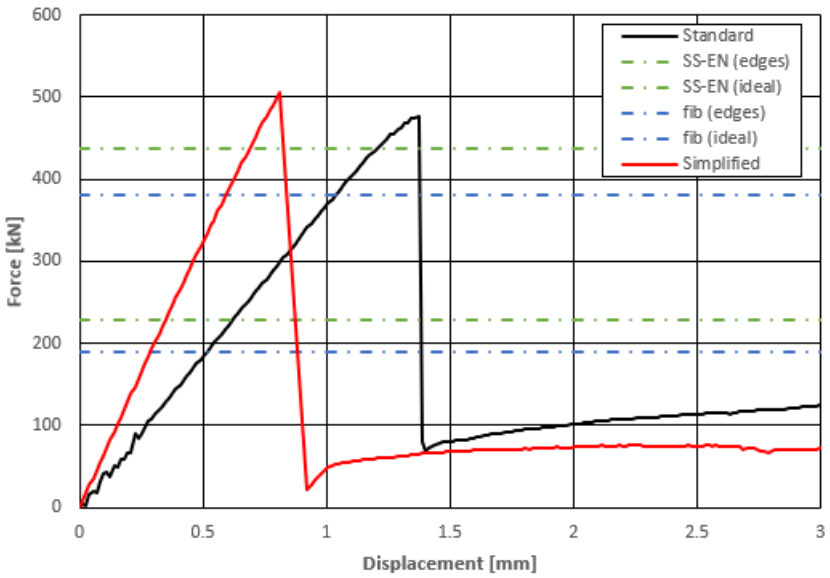

Figure 6.19: Comparision of the two models subjected to tensile loading.

A maximum load of 505 kN is predicted by the model for the narrow corner connection compared to 477 kN for the standard connection, a difference of 28 kN with a percentage value of 5.9%. Maximum load is reached at 0.8 mm for the narrow connection compared to 1.4 mm for the standard connection, a difference of 43% in displacement. Both connections presents a similar pre-failure linear behaviour with little to no indication of plasticity and a brittle failure. The post-failure behaviour also exhibit similar characteristics to each other where the concrete in both connections recovers at 50-70 kN and show a ductile increase of strength.

Relatively small differences in overall behaviour and failure characteristics gives clear indications that no significant changes in failure mode or capacity of the connection have occurred when loaded by a tensile force as a result of the more narrow and asymmetrical design. The moderate difference of 5.9% of maximum load in favour of the narrow connection is well within safety boundaries and could be neglected in design. It's presence could be explain by the implementation of the extra bolt which increases the stiffness in tension, however with the disadvantage of producing a more brittle failure.

Presented in figure 6.20 below is a comparison of the moments in all directions between the standard and narrow corner connection.

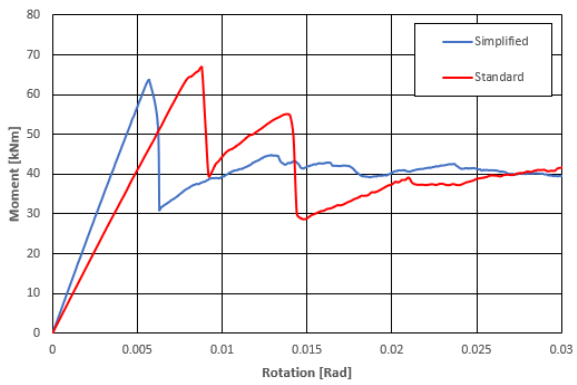

(a) Positive moment

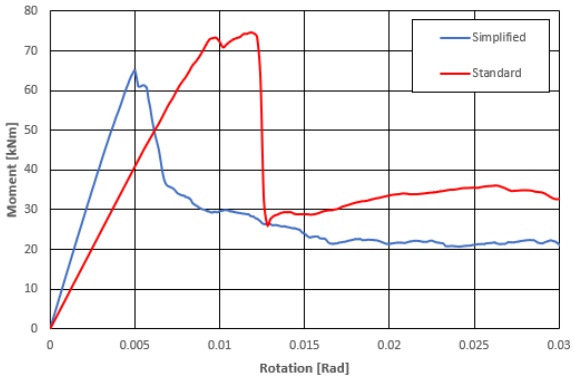

(b) Negative moment

Figure 6.20: Comparison of positive and negative moment along x-axis between narrow corner and standard connection.

When comparing the capacity in the anchors subjected to moment loading some differences and similarities from the model can be observed. The anchors in the standard connection does not fail simultaneously for both moments applied as can be seen from the two knobs post-failure, see red graph 6.20a and 6.20b. For the narrow corner connection, the bolts fails simultaneously for positive moment while a small difference occurs in negative direction. The positive moment is similar for both connections where the maximum moment for the standard connection is 3 kNm larger, a percentage difference of 4.7 %. The difference becomes more evident for negative moment where the difference between the two connections is 8.4 kNm in favour of the standard connection which is a -11.4 % difference.

While the model predicts similar behaviour over both directions for the narrow connection, a difference of this can be observed in the other one. There is a difference in both rotational displacement and moment at the point of failure for the standard connection. Similar for both directions is that the narrow corner connection is more prone to failure at a lower degree of rotation where the difference is 0.0031 rad for the positive direction and 0.007 rad for the negative. This could be explained from a greater stiffness in the narrow connection due to the addition of an extra anchor.

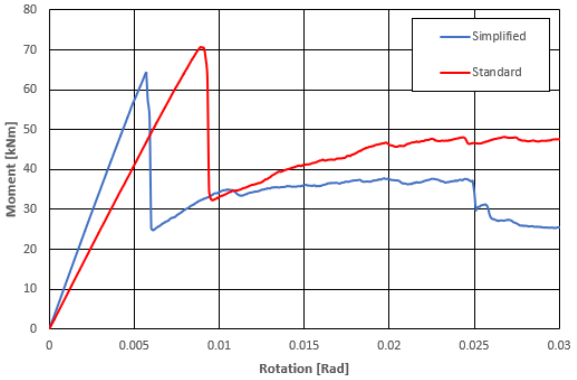

(a) Positive moment

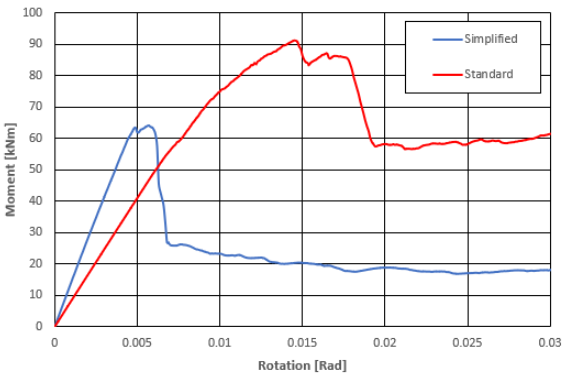

(b) Negative moment

Figure 6.21: Comparison of positive and negative moment along y-axis between narrow and standard connection.

The moment capacity for the y-axis compared between the standard and narrow corner connection is presented in figure 6.21. Similarly to earlier results, these tests show a ductile failure in the negative direction as a result of consecutive failure of individual fasteners. The plastic behaviour exhibited is however significantly more pronounced for the tests around the y-axis than the x-axis and yields significantly larger maximum load. The overcapacity for the negative tests is 42.3% in favour of the standard connection with a 154.4% higher degree of rotation at failure. For the rotation in the positive direction, smaller differences is observed. They also coincide well with those of the x-axis with a maximum load of 71 kN for the standard connection and an under capacity of the narrow connection at -9.3%.

When analyzing all of the graphs in figure 6.20 and 6.21 it is evident that no matter direction of loading the capacity remains in an interval of 64 to 65 kN.

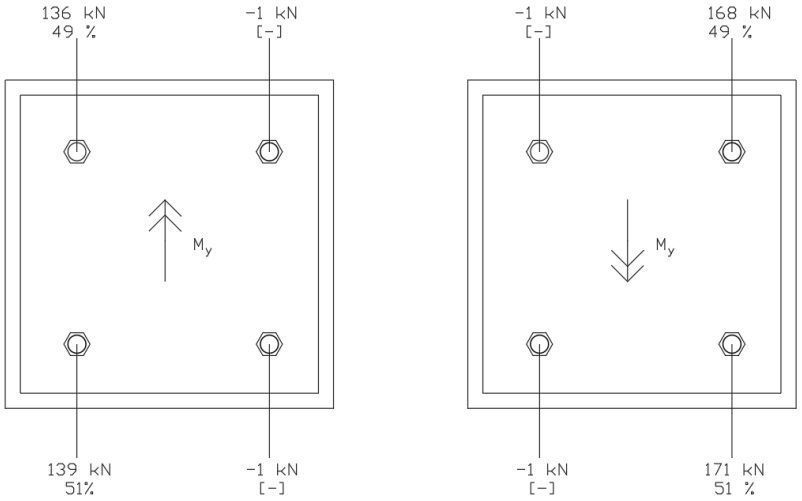

(a) Load distribution for moment along y-axis (left positive, right negative).

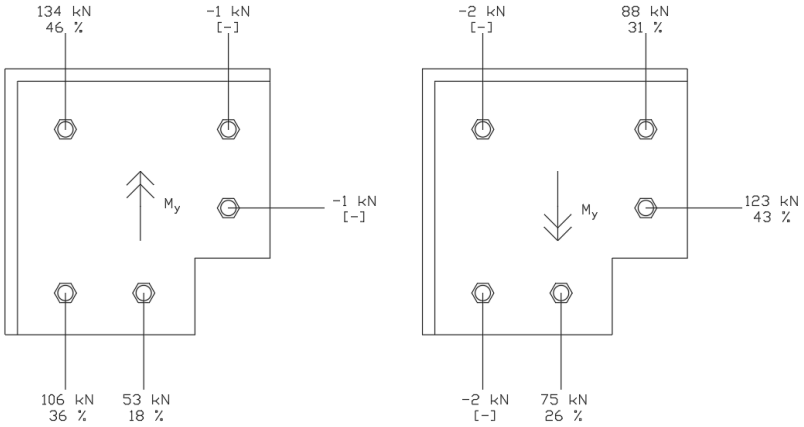

(b) Load distribution for moment along y-axis (left positive, right negative).

Figure 6.22: Comparison of force distribution between standard and narrow corner model for rotation around the y-axis.

By comparing the distribution of forces per bolt at failure for the to connection, as in figure 6.22, it is evident the simplification of calculations has an effect. A difference of 28.1% between the maximum load of the standard and narrow corner model is

observed, mainly due to the uneven distribution of forces concentrating a large load on a single fastener. As shown in the graphs of the overall connection capacity a reduction is achieved and a clearly more brittle behaviour is achieved. This could be the result of the fact that the failure is dependant on only one bolt and its attributed failure mode when a more evenly distributed load give a higher overall concrete strength, providing a ductile failure. The ductile failure is believed to occur in the standard connection due to plastic yielding in the steel bolts.

7 Discussions & Conclusions

In this chapter assumptions made for the model will be discussed as well as conclusions made from the results obtained in chapter 6.

7.1 Finite Element model assumptions

In order to create a reliable model which the users can have a high degree of confident in, it is of utmost importance to prove that the certain model produces correct results usable for the analysis. One way of achieving this is by comparing it to experimental tests in similar circumstances. These circumstances could in this instance be material properties, such as failure of concrete due to compression and tension or a specific load case resulting in certain failure modes. In this instance such a failure mode would most likely be a concrete cone failure. This would verify its applicability for analysis of problems under similar circumstances. A larger number of validation examples would increase the confidence in the model while a lower number of comparison might be sufficient, although with lowered confident in the span of its applicability. The validity of the model in this report could not be deemed sufficient and would need further tests to ascertain a high degree of confident. Instead a calibration of the model was performed by using experimental tests, as described in chapter 5.

Calibration of the model was achieved through the use of experimental tests performed with the aim of producing a concrete cone failure. It was found to correspond reasonable well to the tests, however with a certain degree of error. This indicated that concrete cone failure most probably was the main failure mode achieved in the model and the degree of error could be the result of a number of simplified assumptions made. It must however be noted that the probability for outer failure modes, or a combination of failure mode, to occur could not be excluded. It is most likely that a combination of failure modes would cooperate to achieve failure, especially with varying embedment depth and edge distances. Stress build-up towards the edges, which most reasonable have a high influence due to the short distances, indicate that a combination of failure modes could be a palpable reality. It is, however, only up to the readers own speculation how this would influence the model considering it is only designed for the case of concrete cone failure, the main failure mode. A more comprehensive validation of the model would have to be performed to be able to confidently understand such actions.

Many assumptions were made regarding the Finite Element model and most of them were based upon similar studies that have been conducted previously on the subject. Having the contact properties set as frictionless in the normal direction can be seen as a conservative assumption since there should be friction between the cast-in anchors and the surrounding concrete which should increase the resistance of the connection. As explained before, the lack of friction between the concrete and anchor shank could be one of the reasons for the difference in displacement as seen in figure 5.7. Therefore,

this could influence the deformation observed in the simulations conducted in section 6 which in reality would exhibit a more ductile behaviour with higher deformations. The benefit of this assumption, however, is that all of the force is transferred through the anchor head. This induces concrete cone failure which was the failure mode that was expected to happen due to its low capacity compared to other modes.

Another greatly influential aspect is how the individual parts as well as the connection in general interacts with its surrounding structures. A full model of the entire structure was not practically possible to achieve due to simulation time and complexity. The assumptions made does however produce inaccuracies which must be accounted for in design. The loads are implemented as translational or rotational displacement and does not consider the effects of the steel column on the plate. Local yielding or the effects of bending in the plate not accounted for in this study could result in differently distributed stresses and result in a load case not governed purely by tension in the bolts. The influence on shear on the bolts is a interesting topic not regarded. Beyond the plate and bolt connection, assumptions regarding the plates interaction with the concrete where made which not necessarily coincide with reality. The interaction between plate and concrete was assumed fully in contact without any prior forces acting.

During construction of the connection there are a great risk of imperfections that will influence the connection. This could be the tightness of the applied bolts or the shape of the grout usually found in such a connection. By considering the concrete as uncracked and homogeneous, a risk of achieving higher capacity in the model than reality is created.

Regarding boundary conditions, the assumption was made that the edges in the end of the 700 mm elongation of the concrete was given fixed boundary conditions. The main reason for this was to isolate the structure into a quarter due to different loads. An advantage of this boundary condition is that the model could be isolated to a quarter of the whole structure, saving computational time while retaining the scope of analysing one connection. When not having a fixed boundary condition at the edges, the model produced unrealistic behaviour in the material no matter the time step which reduces the dynamic effects. Simulations were also made giving the outer circumference edges of the concrete fixed boundary conditions, similar to the one for validation model in section 5.2.1. These simulations predicted failure at the fixed edges, a failure mode deemed unrealistic.

Further material assumptions limiting the accuracy of this study is the fact that validation and calibration of the model was conducted using experimental results while using conservative values for all non-concrete parts. This was done based on the assumption that steel influence would be negligible for the specified failure modes researched.

Concrete Damaged Plasticity defines the material model of concrete by applying a multitude of theories in one model. They are implemented through parameters which all contribute to different mechanical behaviour in the concrete when combining the tested data used for creating the model. The validation chapter show that our model with relatively high accuracy simulate real life behaviour of concrete in tension for a selected concrete class. The chosen values for the parameters were however not

all calibrated to this specific instance and could therefore produce a slightly different result. This was however reasoned not to impact the main investigation into the difference between the two models and was therefore neglected.

Uncertainties exist when using an explicit solver for a static problem. The explicit solver does not find static equilibrium for each load increment compared to using a implicit solver. This could lead to larger inaccuracies when the loadings or displacements are applied at higher rates. Quasi-static analysis was achieved by applying the load cases with a low velocity by increasing the step time in ABAQUS. The benefit of this was that the dynamic effects were reduced and a static behaviour could be achieved without having the risk of convergence issues as would have been the case for the implicit solver. However, the need to decrease velocity of the loads came at the cost of computational time due to the complexity and size of the two models. Small dynamic effects could still be observed at simulations which took over 20 hours to compute. By applying the loads at a lower velocity the dynamics effects should disappear. However, since this would increase the computational time to over 30 hours with negligible impact to the results an agreement between dynamic effects and computational time was made.

7.2 Assessment of results

Findings of the analysis shows that going from the standard to the narrow corner connection produces a lower capacity for the connection under certain load cases. The tensile capacity is slightly higher for the narrow connection while the standard connection shows higher capacity for the moment analyses. This difference greatly increases when subjecting the inside part of the connection to tension in the moment analysis. Apart from a higher capacity and larger displacement, the overall behaviour proves much more ductile for the case where three bolts are in tension than for the load case where the two outermost bolts are in tension. This could be the result of increased strength in the concrete due to lower limitations of space for crack propagation leading to a possible yielding in the steel bolts. The more similar to the standard case the configuration of the connection i designed, the more similar behaviour is achieved, as expected. This could be seen when loaded in a positive moment, resulting in only two bolts under tensile loading. To better understand the reason for this, modelling of cracks in the model could be performed by for example displaying the formation of damage within the concrete. Figures displaying stress distribution in the results give a good indication but can not give conclusive evidence to suggest the exact mode of failure.

When determining the concrete cone failure according to design codes, both of the codes tend to heavily underestimate the capacity. Compared to the codes the finite element model is influenced by a compressive zone counteracting the failure of the concrete cone for a bolt in tension. This is accounted for in SS-EN 1992-4 by a factor accounting for a perfectly rectangular compressive zone. The stress distribution does however indicate a more concentrated and irregularly shaped compressive zone.

The assumption that one bolt in the standard connection could be accounted for by an extra bolt in the narrow connection could not be found to hold true. Interestingly it also significantly effected the positive load case which most closely resemble the standard case.

In conclusion, a reduction of capacity in the connection was found when applying the examined change in geometry. This reduction of characteristic resistance for a group of fasteners loaded in tension could be accounted for in design codes using a reduction factor applied for cases with asymmetries. How the implementation of this factor should be achieved to suit a more generalized case could not be conclusively determined by this analysis. It could be problematic to form a reduction factor solely based on a few static load cases with no research into how they interact with each other and other load scenarios.

7.3 Further Research

The authors suggests the following continuations on the master dissertation:

- Combine different static load cases, for example combined tensile and moment loading.
- By performing more extensive research into how the bolts eccentricity affect the connections capacity could prove a more generalize relation between the geometrical asymmetries and reduction of capacity, presenting a basis for design of similar joints with altered design.
- This study was performed exclusively on a single concrete class and the measured values found during specific lab tests. To be able to implement this in more diverse cases a study showing the influence of concrete classes and their attributed strength on the capacity should be performed.
- The influence of reinforcement, both surface and other, was neglected for this study. Investigation of the effects of including reinforcement in similar connections could provide better understanding of the real-life behaviour of this connection and give a better basis of knowledge for future design.
- Conducting laboratory experiments to further study the real life behaviour of the materials.

Bibliography

[1] Robert Eligehausen, Rainer Mallée and John F. Silva. *Anchorage in Concrete Construction*. Ernst and Sohn, 2006.

[2] N.S Trahair and M.A Bradford. *The Behaviour and Design of Steel Structures*. E & FN SPON, 1995.

[3] Tord Isaksson and Annika Mårtensson. *Byggkonstruktion, Regel-och formelsamling*. Studentlitteratur AB, Lund, 2016.

[4] Lennart Elfgren. "Application of fracture mechanics to concrete structures". In: *Proceedings from Workshop on Fracture Toghness and Fracture Energy, Sendai, Japan, October 12-14, 1988* (1988).

[5] Björn Engström. "Kompendium i Betongkonstruktioner". In: *Bärande konstruktioner Del 1* (2013).

[6] Herbert Anton Mang, Roman Lackner, Günther Meschke and J. Mosler. "3.10 – Computational Modeling of Concrete Structures". In: 2003.

[7] Richard Malm. "Predicting shear type crack initiation and growth in concrete with non-linear finite element method". In: 2009.

[8] Rasoul Nilforoush. "Anchorage in Concrete Structures, *Numerical and Experimental Evaluations of Load-Carrying Capacity of Cast-in-Place Headed Anchors and Post-Installed Adhesive Anchors*". PhD thesis. Luleå University of Technology, 2017.

[9] *Eurocode 2 - Design of concrete structures - Part 4: Design of fastenings for use in concrete*. European comitee for standardization, Brussels, 2018.

[10] Niels Ottosen and Hans Petersson. *Introduction to the Finite Element Method*. Ahsford Colour Press Ltd, Great Britain, 1992.

[11] Taylor R. L. Zienkiewicz O. C. *The Finite Element Method*. Whitstable Litho Printers Limited, Great Britain, 1994.

[12] "Dassault Systémes". *"Inelastic behaviour"*. URL: `https://abaqus-docs.mit.edu/2017/English/SIMACAEMATRefMap/simamat-c-plastic.htm`. (accessed: 04.04.2022).

[13] "Dassault Systémes". *"Concrete damaged plasticity"*. URL: `https://abaqus-docs.mit.edu/2017/English/SIMACAEMATRefMap/simamat-c-concretedamaged.htm`. (accessed: 20.03.2022).

[14] A. Hillerborg, M. Modeer and P. E. Petersson. "Analysis of Crack Formation and Crack Growth in Concrete by Means of Fracture Mechanics and Finite Elements". In: *Cement and Concrete Research, vol. 6, pp. 773–782* (1976).

[15] Rasoul Nilforoush and Marjan Shahrokh. "Numerical Evaluation of Structural Behavior of the Simply Supported FRP-RC Beams". PhD thesis. Royal Institute of Technology (KTH), 2012.

[16] Emil Axelsson and Filip Božić. "Numerical analyses of surface reinforcement's impact on anchorage in concrete". PhD thesis. Chalmers University of Technology, 2016.

[17] Daniel Eriksson and Tobias Gasch. "Load capacity of anchorage to concrete at nuclear facilites, *Numerical studies of heades studs and expansion anchors*". PhD thesis. Royal Institute of Technology (KTH), 2011.

[18] *Eurocode 3 - Design of steel structures – Part 1-8: Design of joints.* European comitee for standardization, Brussels, 2005.

[19] *Eurocode 2 - Design of concrete structures – Part 1-1: General rules and rules for buildings.* European comitee for standardization, Brussels, 2005.

[20] Fernando De Abreu Almeida. "The effect of bolt clearance and tolerances on the shear resistance of bolted connections subjected to uni-axial loading, *A parametric study*". PhD thesis. Royal Institute of Technology (KTH), 2018.